iScience

CellPress

Article

The ArfGAP ASAP1 Controls Actin Stress Fiber Organization via Its N-BAR Domain

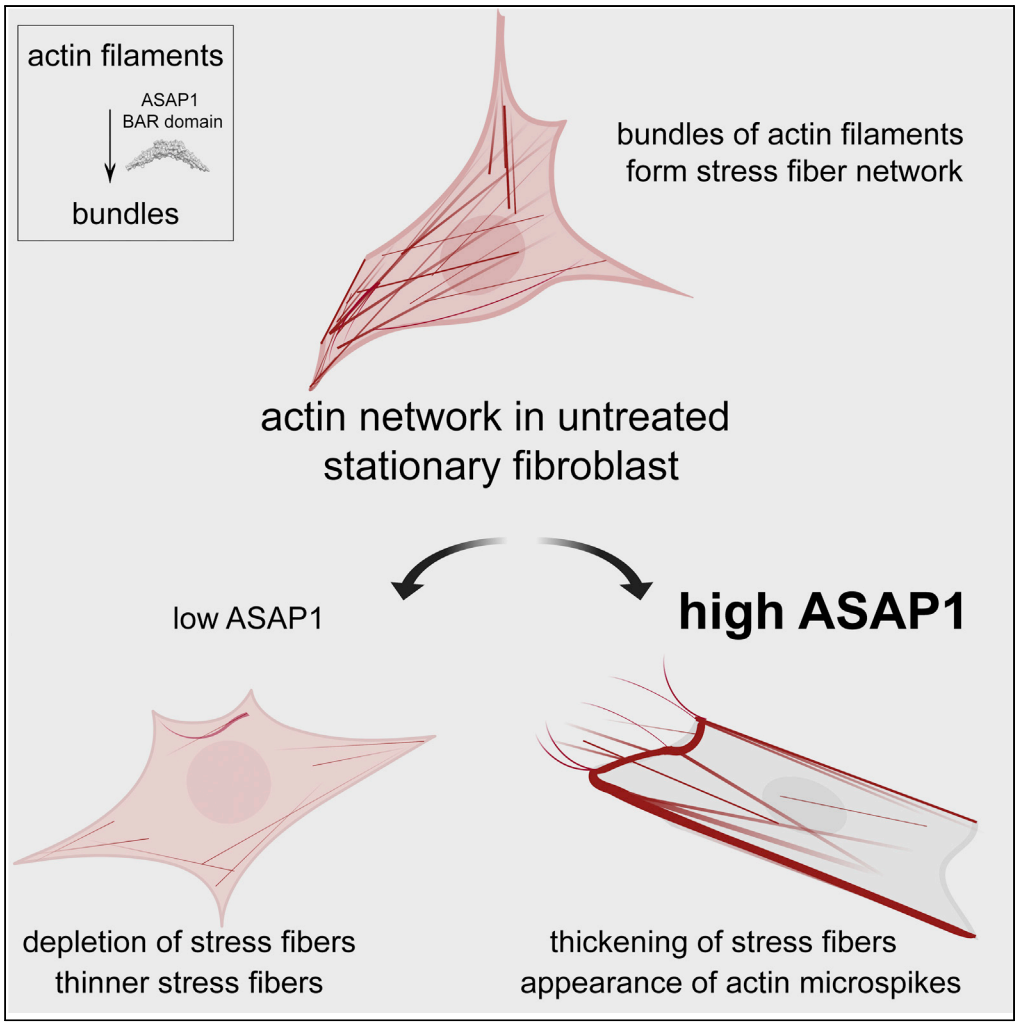

Anjelika Gasilina, Teresa Vitali, Ruibai Luo, Xiaoying Jian, Paul A. Randazzo

randazzp@mail.nih.gov

HIGHLIGHTS

Downregulation of ArfGAP ASAP1 leads to loss of stress fibers

ASAP1 N-BAR domain organizes actin filaments into bundles

Actin bundling by the BAR domain is intramolecularly inhibited by C-terminal domains

Actin remodeling property is not shared with a related ArfGAP ACAP1

Gasilina et al., iScience *22*, 166–180
December 20, 2019
https://doi.org/10.1016/j.isci.2019.11.015

iScience

CellPress

Article

The ArfGAP ASAP1 Controls Actin Stress Fiber Organization via Its N-BAR Domain

Anjelika Gasilina,[1,2] Teresa Vitali,[1,3] Ruibai Luo,[1] Xiaoying Jian,[1] and Paul A. Randazzo[1,4,*]

SUMMARY

ASAP1 is a multi-domain ArfGAP that controls cell migration, spreading, and focal adhesion dynamics. Although its GAP activity contributes to remodeling of the actin cytoskeleton, it does not fully explain all cellular functions of ASAP1. Here we find that ASAP1 regulates actin filament assembly directly through its N-BAR domain and controls stress fiber maintenance. ASAP1 depletion caused defects in stress fiber organization. Conversely, overexpression of ASAP1 enhanced actin remodeling. The BAR-PH fragment was sufficient to affect actin. ASAP1 with the BAR domain replaced with the BAR domain of the related ACAP1 did not affect actin. The BAR-PH tandem of ASAP1 bound and bundled actin filaments directly, whereas the presence of the ArfGAP and the C-terminal linker/SH3 domain reduced binding and bundling of filaments by BAR-PH. Together these data provide evidence that ASAP1 may regulate the actin cytoskeleton through direct interaction of the BAR-PH domain with actin filaments.

INTRODUCTION

Assembly, maintenance, and regulation of the actin cytoskeleton are important for normal cell functions, such as cytokinesis, immune function, morphogenesis, and migration (Gavin, 1999; Wang, 1984; Izdebska et al., 2018; Rougerie et al., 2013; Vonna et al., 2007; Wynn et al., 2013; Blanchoin et al., 2014). Actin dynamics are controlled by an array of actin-regulating proteins (Lappalainen, 2016; Pollard, 2016). Among the diverse families of actin-regulating proteins, the BAR domain proteins have emerged as facilitators of actin filament reorganization. ASAP1, a BAR-domain-containing member of the human ArfGAP family, has been established as a regulator of the actin cytoskeleton and focal adhesion (FA) complexes. Recent observations suggest that regions outside of the ArfGAP domain participate in the regulation of the actin structures (Randazzo et al., 2000; Chen et al., 2016).

In humans, 31 genes encode proteins containing an ArfGAP (ADP ribosylation factor GTPase-activating protein) domain, which stimulates the hydrolysis of the GTP nucleotide by the Arf (ADP-ribosylation factor) GTPases (Kahn et al., 2008). The ArfGAP family has been shown to regulate actin-based structures (reviewed in Tanna et al., 2019). ASAP and ACAP family members are unique in that they contain an N-terminal BAR domain. ASAP1 (also known as DEF1, PAG2, AMAP1, centaurin β4, and DDEF1) is composed of N-BAR, PH, ArfGAP, ankyrin and a stretch of eight E/DLPPKP repeats, a proline-rich domain, and SH3 domains. It was first discovered on the basis of GAP activity and for binding Src and later, as a differentiation enhancement factor (Bharti et al., 2007; Brown et al., 1998; King et al., 1999). ASAP1 affects processes in normal cells, such as neurite outgrowth, and in diseases, such as uveal melanoma and colorectal, prostate, breast, and head and neck cancers (Inoue et al., 2008; Mazelova et al., 2009; Wang et al., 2012; Muller et al., 2010; Ehlers et al., 2005; Sato et al., 2014; Lin et al., 2008; Li et al., 2018).

In addition to Src, it binds the oncogenes CrkL, FAK, and cortactin. ASAP1 localizes to the FAs via its interaction with focal adhesion kinase (FAK) and adapter protein CrkL and to the membrane ruffles through CD2AP (Randazzo et al., 2000; Liu et al., 2002, 2005; Oda et al., 2003). ASAP1 has been shown to regulate podosome and invadopodia formation (Yonenaga et al., 2005; Onodera et al., 2005). The BAR domain of ASAP1 induces membrane tubulation, as described for many other BAR domain-containing proteins (Nie et al., 2006). Downregulation of ASAP1 expression in rat fibroblasts inhibits cell migration and impedes cell spreading (Liu et al., 2005), whereas in NIH 3T3 fibroblasts and HeLa cells, knockdown of ASAP1 accelerates cell migration and cell spreading (Chen et al., 2016).

The BAR domain superfamily is composed of four subfamilies—BAR, N-BAR (previously clustered together with BAR), F-BAR, and I-BAR. BAR domain proteins have additional domains—catalytic, lipid-binding, or

[1]Section on Regulation of Ras Superfamily, Laboratory of Cellular and Molecular Biology, Center for Cancer Research, National Cancer Institute, National Institutes of Health, Bldg. 37, Rm. 2042, Bethesda, MD 20892, USA

[2]Department of Biochemistry and Molecular & Cellular Biology, Georgetown University Medical Center, Washington, DC 20007, USA

[3]Present address. Department of Molecular & Integrative Physiology, University of Michigan Medical School, Ann Arbor MI 48109, USA

[4]Lead Contact

*Correspondence: randazzp@mail.nih.gov

https://doi.org/10.1016/j.isci.2019.11.015

protein-protein interaction domains—which may also serve as regulatory elements to control the localization and activity of the BAR domain (reviewed in Carman and Dominguez, 2018). N-BAR domain protein BIN1 (amphiphysin II) has been shown to directly organize actin filaments into bundles and stabilize tau-induced actin bundles via its BAR domain, which may affect neuronal functions, such as those dysregulated in Alzheimer disease (Drager et al., 2017; Lasorsa et al., 2018; Calafate et al., 2016). A member of the F-BAR domain family, PACSIN2 (syndapin II), has also been shown to directly bind actin filaments and is important for maintenance of the adherens junctions in endothelial cells (Kostan et al., 2014; Dorland et al., 2016). The I-BAR domain family members (MIM) Missing-in-Metastasis and IRSp53 have been shown to bundle actin *in vitro* and induce formation of filopodia (Nakagawa, 2003; Yamagishi et al., 2004; Millard et al., 2005; Lee et al., 2007). Members of the BAR superfamily thus stand at the crossroads of cellular signaling, membrane, and cytoskeletal dynamics.

Actin filaments take on multiple forms, one of them being actin stress fibers. There are three major types of stress fibers—ventral stress fibers (VSFs), dorsal stress fibers (DSFs), and transverse arcs (TAs). Stress fibers participate in dynamic processes during cell migration and adhesion to substratum and are assembled via different mechanisms (Hotulainen and Lappalainen, 2006; Tojkander et al., 2011, 2012, 2015). VSFs and DSFs are anchored to FAs—VSFs anchor at both ends and DSFs anchor at one end only. They also differ in location, orientation, and composition, with VSFs rich in non-muscle myosin 2, and DSFs having little detectable NM2. TAs are prominent in actively migrating and spreading cells and do not associate with FAs, but rather extend to the DSFs. TAs and DSFs may combine to form VSFs (Kovac et al., 2013; Vallenius, 2013).

Recently, we have determined that the BAR-PH region of ASAP1 binds non-muscle myosin 2A (NM2A), ASAP1 and NM2A colocalize at circular dorsal ruffles upon mitogen stimulation, and downregulation of ASAP1 leads to disruption in actin and NM2A colocalization (Chen et al., 2016). The proteomics screen that was used to identify non-muscle myosin 2A also identified actin as a putative binding partner of the BAR-PH region. We have additionally detected irregular F-actin staining in the fibroblasts depleted of ASAP1. The emerging field of the BAR-domain superfamily as actin regulators has led us to hypothesize that ASAP1 could also be directly involved in the assembly or maintenance of actin structures. As ASAP1 contributes to FA assembly and regulates association of NM2A with actin filaments, we focused on the VSFs as a model of bundled actin filaments. We chose mouse NIH 3T3 and primary human foreskin fibroblasts (HFFs), which contain prominent VSFs, as cell models to study the role ASAP1 may play in the regulation of actin structures. Our biochemical and cell biological data indicate that the N-BAR domain of ASAP1 directly binds and bundles actin filaments and regulates dynamic actin structures.

RESULTS

Depletion of ASAP1 Leads to Loss of Ventral Stress Fibers and Perturbs Levels of Filamentous Actin in Fibroblasts

We have previously observed that the knockdown of ASAP1 in NIH 3T3 fibroblasts leads to reduced colocalization of NM2A and F-actin (Chen et al., 2016). In cells with reduced expression of ASAP1, the morphology appeared irregular with presence of thinner, misaligned stress fibers compared with cells with unaltered ASAP1 levels. To further evaluate the effect of ASAP1 on actin stress fibers, we transiently transfected mouse NIH 3T3 fibroblast and primary HFF-1 cells with two independent control and ASAP1 small interfering RNAs (siRNAs), re-plated the cells on fibronectin in serum-free media for 5.5 h, stained with fluorescently labeled phalloidin, and examined single cells using confocal microscopy. Total phalloidin fluorescence intensity, a readout of total filamentous actin content in the cell, as well as the phalloidin intensity of the ventral portion, decreased by 20%–30% in NIH 3T3 cells (Figures 1A–1C) and 30%–40% in HFF-1 cells transfected with ASAP1 siRNA (Figures S1A–S1D). We then extracted and stained stress fibers attached to the fibronectin matrix from the HFF-1 cells to observe changes in VSF organization (Katoh et al., 2000; Eltzner et al., 2015). Cells transfected with ASAP1 siRNA had fewer VSFs than the control or mock-treated cells, as indicated by the red asterisks in Figure 1D. Total phalloidin fluorescence quantification confirmed that the ASAP1-depleted cells had less filamentous actin (Figure 1E) and fewer stress fibers than the control cells (Figure 1F). In addition, we used immunoblotting-based analysis (see *In Vivo* F-Actin/G-Actin Assay in Materials and Methods) to probe for changes in the ratios of globular and filamentous actin. NIH 3T3 fibroblasts were transfected with control or ASAP1 siRNA for 72 h (ASAP1 expression is shown in Figure 1G), plated in fibronectin-coated plates for 5.5 h, lysed in F-actin stabilization buffer, and subjected to high-speed centrifugation at 100,000 × *g* for 1 h at 37°C to separate actin filaments (pellet, P)

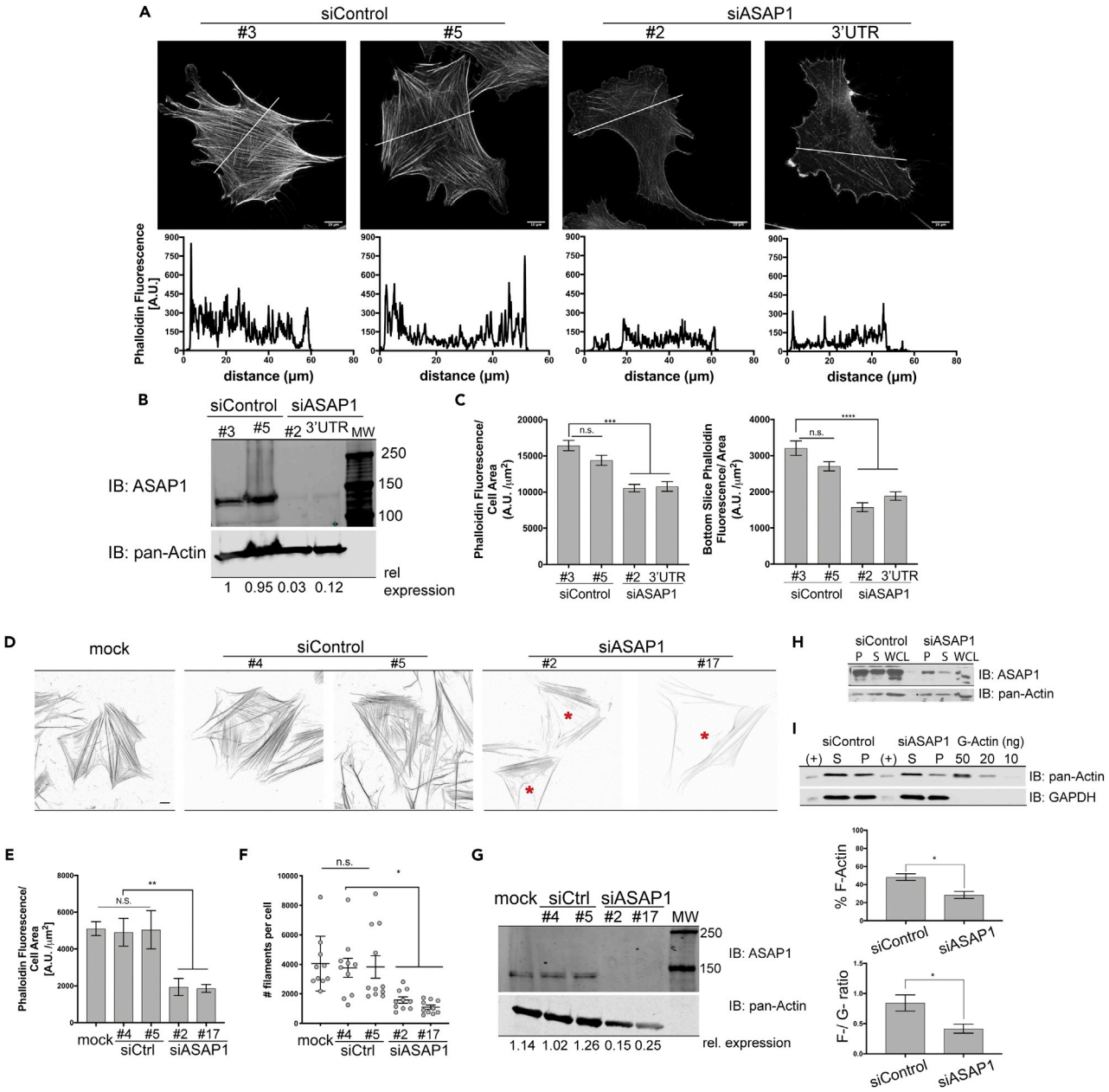

Figure 1. Reduced Expression of ASAP1 Decreases the Levels of Filamentous Actin and Affects Distribution of Stress Fibers in Primary Foreskin and 3T3 Fibroblasts

(A–C) Effect of ASAP1 on actin in mouse NIH 3T3 fibroblasts. NIH 3T3 fibroblasts were transiently transfected with two independent control or ASAP1 siRNAs; 72 h post-transfection, cells were re-plated on fibronectin-coated coverslips for 5.5 h, fixed, and stained with phalloidin Alexa Fluor 488. Single-cell z stack images were acquired on a Leica SP8 confocal microscope using 63× oil objective. (A) Representative maximum intensity projections (MIPs) of F-actin stained with phalloidin Alexa Fluor 488 control and ASAP1-depleted 3T3 cells are shown. Line scans of fluorescence intensity perpendicular to the visualized stress fibers (white lines in images) of the sum of stacks are presented below the images. Scale bar, 10 µm. (B) ASAP1 levels in siRNA-transfected cells. ASAP1 in cells lysates was determined by quantitative immunoblotting. (C) Cellular content of F-actin. Relative F-actin content in cells was determined by quantifying phalloidin fluorescence, n = 15. Results are presented as total surface fluorescence divided by cell area (left panel) or fluorescence of the bottom cell slice only divided by the area (right panel) with the units being arbitrary fluorescence units (AU)/µm^2 and representative of three independent experiments. See also Figure S1.

(D–G) Effect of ASAP1 on actin in primary human foreskin fibroblasts (HFF-1). HFF-1s were mock treated or transiently transfected with two independent control or ASAP1 siRNAs. Post-transfection, cells were re-plated on fibronectin-coated coverslips, followed by stress fiber extraction. Isolated stress fibers were fixed and stained with phalloidin Alexa Fluor 488. (D) Representative MIP images. LUTs (look-up tables) were inverted in Fiji and contrast enhanced equally across all images. Scale bar, 10 µm. Red asterisks indicate lack of substratum-attached stress fibers in siASAP1 cells. (E) Actin content in transfected

Figure 1. *Continued*

HFF-1 cells. Filamentous actin content in extracted cells was quantified as total cell fluorescence on sum of stacks per cell area; 10 cells for each condition were analyzed. (F) Estimate of number of stress fibers in transfected HFF-1s. (G) ASAP1 levels in transfected HFF-1s. ASAP1 levels were determined as described for Figure 1B.

(H and I) Effect of ASAP1 knockdown on F-actin content of NIH 3T3 fibroblasts. NIH 3T3 fibroblasts were transfected as previously described and processed with *in vivo* actin assay kit to assess F-actin and G-actin content by immunoblotting. (H) ASAP1 levels in the siRNA-transfected cells. ASAP1 levels were determined by immunoblot. (I) Relative F- and G-actin content of cells. Quantitative immunoblots of cellular fractions containing F- and G-actin, as indicated, from control and ASAP1 siRNA-treated cells are shown. The percentage of filamentous actin (% F-Actin) and F- to G-actin ratios were calculated and the summary of 5 combined experiments is presented in the bar graphs below the blots. S, supernatant; P, pellet; WCL, whole-cell lysate; (+), positive immunotransfer control G-actin standard.

Quantifications represented as mean ± SEM, *$p < 0.05$, **$p < 0.01$, ***$p < 0.001$, n.s., not significant.

and globular actin (supernatant, S). Consistently with immunofluorescence (IF)-based assays, immunoblotting-based analysis showed 40% decrease in filamentous actin content (% F-actin) of 3T3 cells (48% ± 4% in control cells versus 28% ± 4% in siASAP1 cells) and ratio of filamentous to globular actin (F-/G-ratio) reduced from 0.84 ± 0.13 in control cells to 0.41 ± 0.07 in knockdown cells (Figures 1H and 1I). Thus, ASAP1 is important for maintaining cellular filamentous actin levels and VSF network.

ASAP1 Remodels Actin in Fibroblasts, Binds to and Bundles Actin Filaments *In Vitro*, and the C Terminus of ASAP1 Modulates N-BAR-Mediated Actin Binding and Bundling Activity

We next examined the effect of overexpression of ASAP1 on the filamentous actin content and stress fibers. We transiently transfected NIH 3T3 cells with FLAG-tagged full-length or domain truncations of ASAP1 (see Figure 2A for domain boundaries and nomenclature), re-plated cells on fibronectin in serum-free media for 5.5 h, stained with fluorescent anti-FLAG antibody and phalloidin, and examined cells using confocal microscopy (representative images shown in Figure 2B). Quantification of total phalloidin fluorescence indicated that only constructs containing the BAR-PH tandem led to the increase of filamentous actin content (Figure 2C). We did not observe any differences in phalloidin fluorescence intensity between BAR-PH, BARPZA (BAR-PH-GAP-Ank), and the full-length ASAP1. We also observed similar phalloidin fluorescence intensity between low-, mid-, and high-full-length ASAP1-expressing cells (Figure S2A). Phalloidin staining also revealed multiple actin microspikes and protrusions in cells expressing ASAP1 BAR-PH (Figure 2D), whereas overexpression of BARPZA and the full-length ASAP1 protein had lower number of cells with actin protrusions (30% and 17%, respectively, compared with 70% of BAR-PH-expressing cells). In addition, we observed that cells expressing the BAR-PH and BARPZA have a collapsed, elongated cell shape (Figure 2E), and BAR-PH-expressing cells have a reduced cell area (Figure 2F).

We have previously observed that ASAP1 loss leads to decrease in number of mature adhesions and stress fibers are known to guide maturation of FAs (Chen et al., 2016; Oakes et al., 2012). Co-staining of BAR-PH- and ΔBAR-PH-expressing 3T3 fibroblasts with paxillin, an FA marker, revealed subcellular localization of ΔBAR-PH, but not BAR-PH, to immature adhesions (Figure S2B).

The observation that overexpression of ASAP1 BAR-PH leads to reorganization of actin stress fibers and formation of actin microspikes in cells led us to hypothesize that direct interaction between the BAR-PH tandem of ASAP1 and actin filaments mediates actin remodeling. To determine if ASAP1 binds directly to actin and to dissect the region that binds to filaments, we purified recombinant full-length and fragments of ASAP1 (see Figure S3A for protein purity) and performed binding assays using high-speed actin co-sedimentation. Purified ASAP1 and ASAP1 fragments, as well as negative (BSA) and positive (α-actinin) controls, at 2 μM, were incubated with increasing (0–25 μM) concentrations of F-actin for 30 min at room temperature in F-actin buffer and subjected to high-speed centrifugation at 150,000 × *g* for 1.5 h at 23°C to pellet actin filaments and proteins bound to filaments. Pellet (actin filaments and bound proteins) and supernatant (unbound proteins and residual G-actin) fractions were resuspended in an equal volume of Laemmli sample buffer and resolved on SDS-PAGE. Pellet fractions were analyzed as a percentage of total (pellet/(supernatant + pellet)) and plotted for all proteins examined (Figure 3K). The majority of actin was in the filamentous form (Figure 3A). We observed that, similar to the positive control α-actinin (Figure 3B), ASAP1 BAR-PH bound to actin filaments in a concentration-dependent manner (Figure 3C). PZA, the fragment that contains the PH domain, but lacks the BAR domain, did not co-sediment with actin filaments, suggesting that the BAR domain is the actin-binding module in the BAR-PH tandem (Figure 3D). ASAP1 BARPZA, and FL, which in addition to the BAR-PH have the GAP and ANK repeats and GAP, ANK, and PXXP, E/DLPPKP, and SH3 domains, respectively, bound less efficiently. Forty-two percent and 43% of

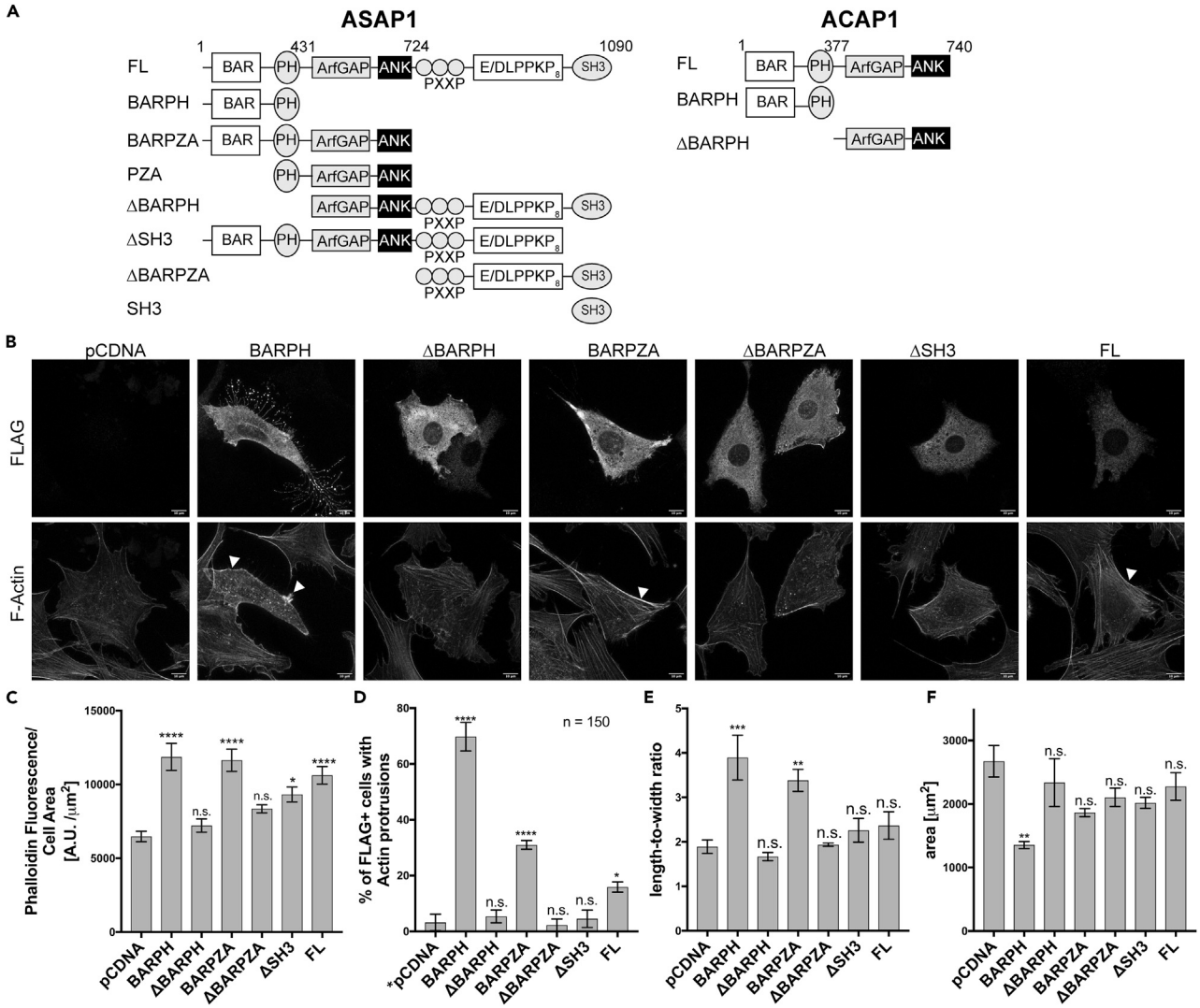

Figure 2. Overexpression of the BAR-PH Tandem of ASAP1 Induces Aberrant Actin Protrusions and Increases Filamentous Actin Content in NIH 3T3 Fibroblasts

(A) Domain architecture of ASAP1 and ACAP1. Schematics of the full length and recombinant proteins are shown. BAR, Bin/Amphiphysin/Rvs; PH, Pleckstrin Homology; ArfGAP, Arf GTPase-activating protein; ANK, ankyrin repeat; PXXP, proline-rich motif; E/DLPPKP, a stretch of eight repeats of E/DLPPKP; SH3, Src homology 3 domain.

(B–F) Effect of BAR-PH tandem overexpression on actin in NIH 3T3 fibroblasts. NIH 3T3 cells were transiently transfected with empty pCDNA vector or FLAG-tagged full-length or domain truncations of ASAP1, re-plated after 24 h on fibronectin-coated coverslips, fixed, and stained with anti-FLAG antibody (Alexa Fluor 488) and fluorescently labeled phalloidin (Alexa Fluor 594). Images were acquired as described for Figure 1. (B) Images of cells overexpressing the BAR-PH tandem. Representative MIPs of the FLAG channel (recombinant ASAP1 protein, upper panels) and phalloidin channel (actin, lower panels) are shown. White arrowheads point to areas of thickened cortical actin. Scale bar, 10 μm. (C) F-actin content of cells expressing ASAP1 and fragments of ASAP1. Phalloidin fluorescence was used as a measure of filamentous actin as described in Figure 1. See also Figure S2. (D) Effect of ASAP1 and domain fragments of ASAP1 on actin protrusions. The percentage of FLAG-positive cells with actin protrusions is presented. Random empty vector cells were counted for presence of protrusions as the control. (E) Effect of expression of ASAP1 and domain fragments on cell shape. Length-to-width ratios were determined as described in Figure 1. (F) Effect of overexpression of ASAP1 and domain fragments on cell area. Cell area was determined as described for Figure 1. A representative experiment of three independent experiments is shown. The data are summarized as means ± SEM, for (C, D, and F); 15 cells were analyzed for each condition. The data were analyzed with one-way ANOVA followed by multiple comparisons using the Tukey's post hoc test, in which all conditions were compared to the pCDNA control, *p < 0.05, **p < 0.01, ***p < 0.001, ****p < 0.0001.

BARPZA and FL proteins were found in the pellet, respectively (Figures 3E and 3F). There was no detectable binding of ΔBARPZA, which only contains PXXP, E/DLPPKP, and SH3 domains, to actin (Figure 3G). The isolated SH3 domain, likewise, did not bind actin filaments (GST-SH3) (Figure 3H). Neither GST nor BSA bound

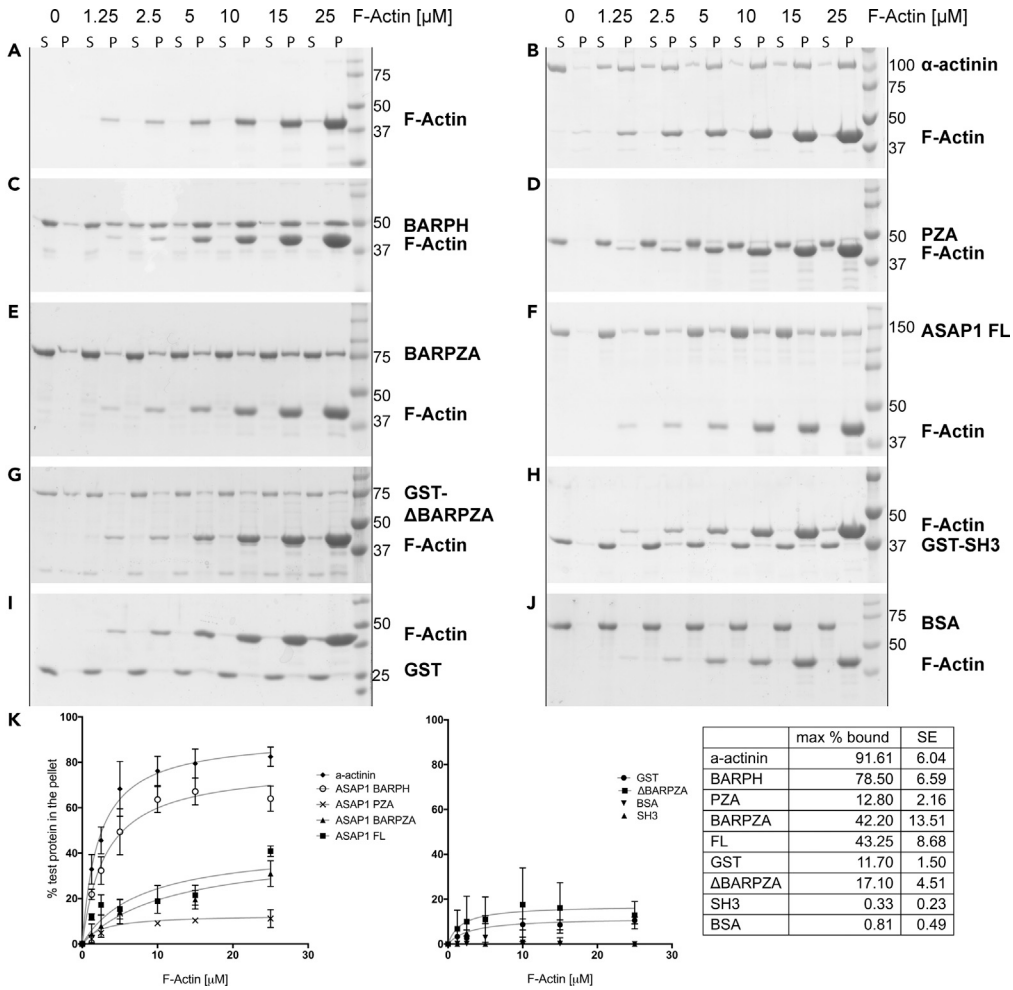

	max % bound	SE
a-actinin	91.61	6.04
BARPH	78.50	6.59
PZA	12.80	2.16
BARPZA	42.20	13.51
FL	43.25	8.68
GST	11.70	1.50
ΔBARPZA	17.10	4.51
SH3	0.33	0.23
BSA	0.81	0.49

Figure 3. ASAP1 Binds Directly to Actin Filaments through Its N-BAR Domain

(A–J) Purified recombinant ASAP1 full-length and domain fragments (2 μM) were subjected to high-speed co-sedimentation assay with the indicated concentrations (0–25 μM) of rabbit muscle F-actin. Actin filaments and filament-bound proteins (P, pellet) were separated from residual globular actin and unbound proteins (S, supernatant), resolved on single percentage (10 or 12%) SDS-PAGE, and stained with GelCode Blue. Co-sedimentation with BSA and GST (negative controls) and α-actinin (positive control) was performed in the same fashion. F-actin was titrated into solutions containing (A) no additional proteins, (B) α-actinin, (C) ASAP1 BAR-PH, (D) PZA, (E) BARPZA, (F) full-length ASAP1, (G) GST-ΔBARPZA, (H) GST-SH3, (I) GST, and (J) BSA. Gels are representative of at least three independent experiments.

(K) Summary of quantification of binding for 3 experiments. The extent of binding to actin was calculated as the percentage of total protein in the pellet, e.g., ASAP1 in P/(ASAP1 in P + ASAP1 in S) × 100%, and plotted against the concentration of actin. Data from three independent experiments were combined, and each point on the graph is a mean ± SEM. Table (right) summarizes the estimated % maximum bound of each test protein with standard error (SE) at saturating actin concentration.

to BAR-PH (Figures 3I and 3J). The results from the high-speed actin co-sedimentation assay (summarized in the table) thus indicate that the BAR domain of ASAP1 binds to actin filaments *in vitro*.

Protease protection was used as a complementary approach to assess binding of ASAP1 to actin filaments. Subtilisin A is a commonly used protease to study protein interactions with filamentous actin, because unlike globular actin, filamentous actin is not susceptible to degradation by subtilisin A (Fievez and Carlier, 1993). We reasoned that interaction with actin filaments will protect ASAP1 from proteolytic degradation by subtilisin A. ASAP1 (1 mg/mL) and F-actin (0.5 mg/mL), incubated together or alone under similar conditions as those used for co-sedimentation, were treated with subtilisin A (0.1 μg/mL) for the duration indicated in Figure 4. A parallel experiment with globular actin (G-actin) in place of F-actin was performed in a

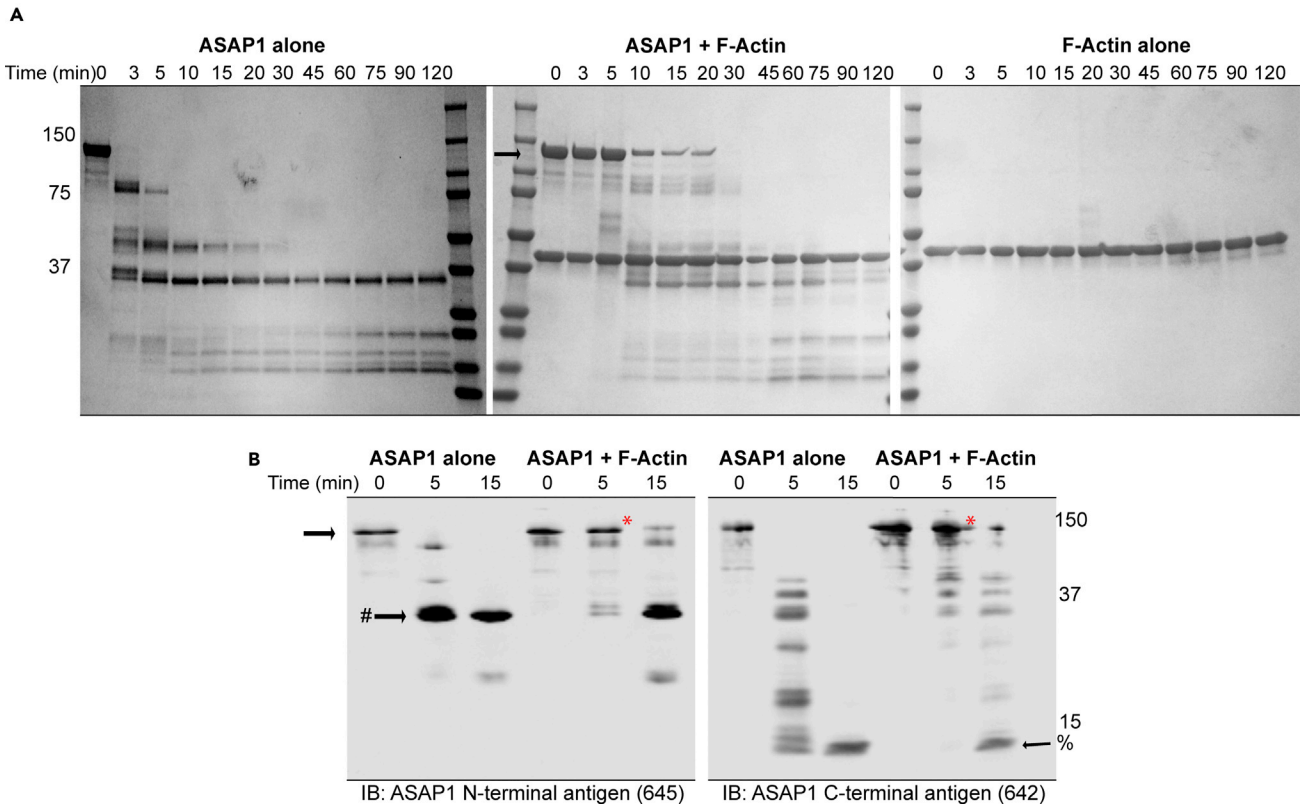

Figure 4. ASAP1 Binding to F-Actin Assessed by Limited Proteolysis

Recombinant WT ASAP1 FL (1 mg/mL) was incubated with F-actin (0.5 mg/mL) in the F-buffer for 30 min and incubated with subtilisin A (0.1 μg/mL). ASAP1 and F-actin alone were used as controls. Aliquots from the proteolysis reactions were taken at the indicated times.

(A) Examination of total protein. Aliquots removed from the incubation were analyzed by SDS-PAGE followed by staining for proteins with GelCode Blue. Representative gels of ASAP1 alone (left), ASAP1 with F-actin (middle), or F-actin alone (right) are shown. See also Figure S3B.

(B) Protein fragmentation pattern analyzed by immunoblot. Aliquots from 0, 5, and 15 min time points were separated on 12% SDS-PAGE in duplicates, transferred onto the nitrocellulose membrane, and each half was probed with an antibody against the N- (645, left) or C-terminal (642, right) region of ASAP1. Full-length ASAP1 is indicated with black arrows and red asterisks. The major proteolytic products detected with the antibody to the N terminus are indicated with the black arrow with a # sign. The major proteolytic products detected with the antibody to the C terminus are indicated with the black arrow with a % sign.

similar manner (Figure S3B). Incubation of ASAP1 alone with subtilisin A led to conversion of the protein into lower-molecular-weight products after 3 min (Figure 4A, left gel). When ASAP1 was pre-incubated with F-actin, digestion of the full-length ASAP1 band (black arrow) was slowed, with loss of full-length ASAP1 requiring 20 min (middle gel). F-actin was resistant to proteolysis, as reported in the literature (right gel). G-actin did not affect the rate of ASAP1 proteolysis (Figure S3B). To assess which region is protected from subtilisin A degradation by F-actin binding, 0-, 5-, and 15-min aliquots were subjected to quantitative immunoblotting using antibodies against N- and C-terminal antigens of ASAP1. We confirmed that full-length ASAP1 is protected at 5 min in the presence of F-actin (red asterisk) when compared with ASAP1 alone. Using the antibody to the N terminus, a proteolytic product around 37 kDa was detected at 5 min in the absence of F-actin. In the presence of F-actin, the rate of generation of the 37-kDa product was slowed, with a faint signal at 5 min and a robust signal after 15 min of protease treatment (Figure 4B). In the blot using the antibody to the C terminus of ASAP1, protease products forming a ladder-like signal were detected after 5 min of subtilisin A treatment. Including F-actin with ASAP1 diminished the laddering, even at the longest treatment interval examined, 15 min. These results suggest that both termini of ASAP1 are protected from protease degradation in the presence of actin filaments.

The *in vitro* biochemical data indicated that ASAP1 interacts directly with actin filaments and experiments in cells are consistent with the idea that ASAP1 controls stress fibers. Actin structures, such as stress fibers and microspikes, are made up of F-actin bundles, which are cross-linked aligned actin filaments. ASAP1 is a

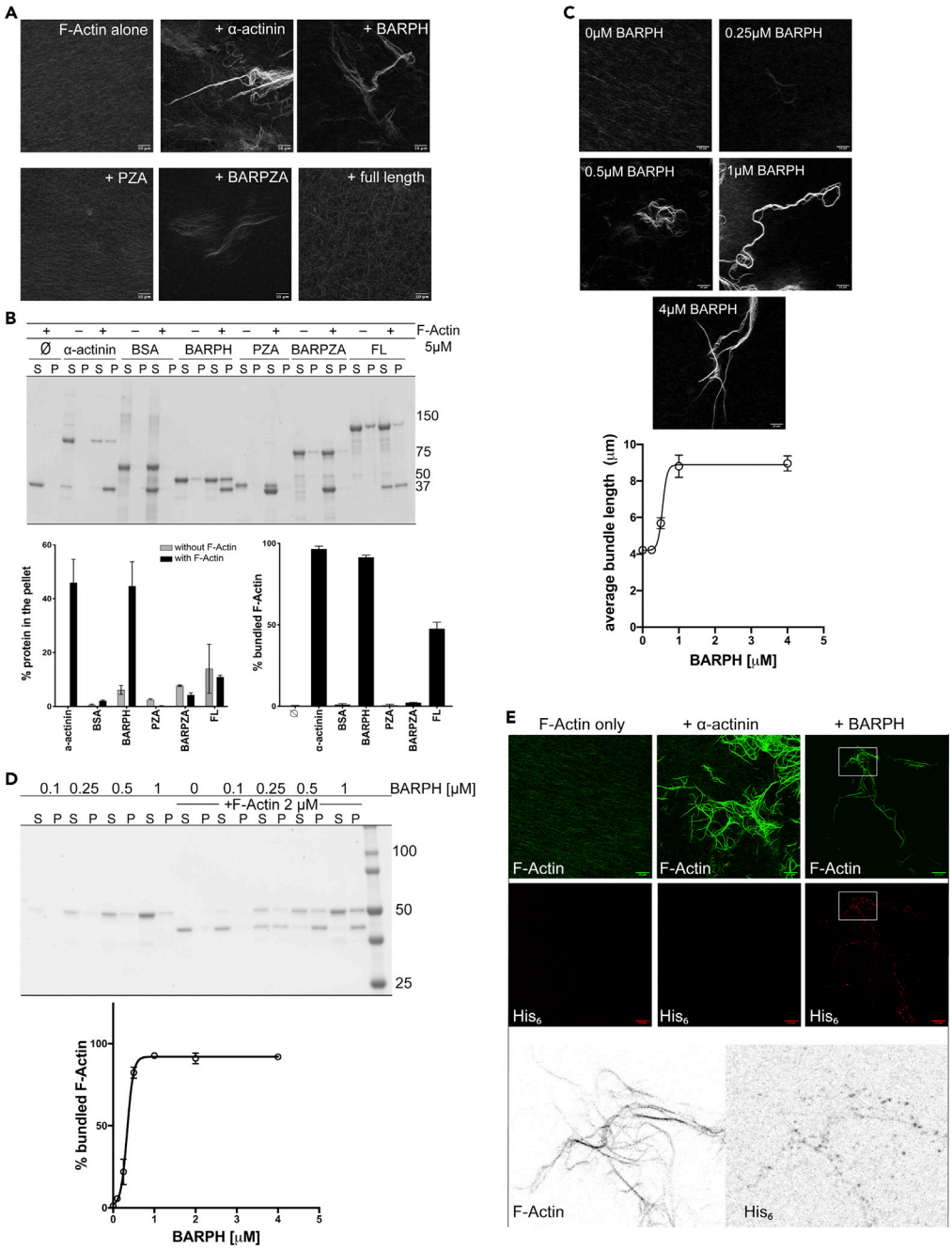

Figure 5. ASAP1 Bundles Actin Filaments *In Vitro* through Its N-BAR Domain and the C Terminus of ASAP1 Negatively Modulates the Bundling Activity

(A) Effect of ASAP1 on bundling of F-actin assessed by fluorescence microscopy. Rabbit muscle F-actin (3.3 μM) alone or with ASAP1, the indicated truncations of ASAP1, or α-actinin (positive control) (3.3 μM) were mixed in F-actin buffer and spotted on poly-L-lysine-coated coverslips. After 30 min, coverslips were fixed and stained with rhodamine phalloidin. Images were taken on Leica SP8 confocal microscope using 63× oil objective. Representative maximum intensity projection images are shown, scale bar, 10 μm. Data are representative of 5 independent experiments.

(B) Effect of ASAP1 on bundling of F-actin assessed by a low-speed co-sedimentation assay. F-actin (5 μM) alone, ASAP1 or ASAP1 truncations or α-actinin alone (2 μM), or F-actin with the indicated proteins were subjected to low-speed co-sedimentation assay. Equal volumes of the supernatant (S) and resuspended pellet (P) were resolved on gradient SDS-PAGE and stained with GelCode Blue. A gel representative of three experiments is shown in the upper panel. In the lower left panel, the percentage of the indicated proteins that sedimented in the absence and presence of F-actin, calculated

Figure 5. *Continued*

from three experiments, is shown. In the right lower panel, the percentage of F-actin that sedimented in the presence of the indicated proteins is shown. The means ± SEM from three experiments are presented. See also Figures S4A–S4C.

(C) Effect of BAR-PH and length of F-actin bundles. F-actin (1 μM) was incubated with the indicated concentrations of BAR-PH and subjected to IF-based bundling assay as in (A). Filament length was approximated using the ridge plugin in Fiji/ImageJ. Results are representative of three independent experiments. Results are summarized as the mean ± SEM, Scale bar, 10 μm.

(D) Bundling efficiency of BAR-PH. The percentage of F-actin bundled at different concentrations of BAR-PH was determined by the sedimentation assay. Increasing concentrations of BAR-PH (0.1–4 μM) were titrated into a solution containing a fixed concentration of F-actin (2 μM) and incubated for 30 min at 23°C. Actin bundles were separated from free filaments by centrifugation at 14,000 × *g* for 30 min. A representative gel is shown in the upper panel. A summary of the combined results of three experiments is shown in the lower panel. The mean % bundled F-actin ± SEM at each BAR-PH concentration is presented.

(E) Incorporation of BAR-PH into actin bundles. Colocalization of BAR-PH with actin bundles was assessed by immunofluorescence. F-Actin alone (1 μM), with α-actinin (1 μM, tagless), as a positive actin-bundling control, or with ASAP1 BAR-PH (1 μM, His_6-tagged) was incubated as in (A) and double-stained for F-actin (phalloidin Alexa Fluor 488) and His_6-tag (goat anti-mouse Alexa Fluor 594) and analyzed by microscopy as in (A). A single Z-slice for each condition is shown, brightness and contrast are enhanced equally for presentation purposes, scale bar, 10 μm. As α-actinin does not have a His_6 tag, there was no signal in the His_6 channel under this condition. Areas shown in white rectangles were enlarged with LUTs inverted to reveal puncta.

homodimer, so it may be able to bind two actin filaments simultaneously. These results taken together led us to hypothesize that the BAR domain of ASAP1 may bundle actin. We used two independent assays to assess bundling activity of ASAP1—a fluorescence-based actin-bundling assay, wherein actin bundles can be examined by staining with fluorescent phalloidin, and a low-speed co-sedimentation assay, wherein actin filaments cross-linked by a bundling protein sediment at a low speed (10,000–14,000 × *g* range) (Yamada et al., 2013, 2016; Lin-Jones and Burnside, 2007). As shown in Figures 5A, 5B, and S4A–S4C, BAR-PH region induced thick actin bundles similar to α-actinin, a known actin-bundling protein, whereas BARPZA and full-length proteins, which have a reduced actin binding, did not bundle F-actin efficiently as determined by fluorescence microscopy and no F-actin bundling was detected by the low-speed co-sedimentation assay. PZA, which does not bind actin filaments, had no actin-bundling activity. We next tested BAR-PH actin bundling at different concentrations of BAR-PH. As shown in Figures 5C and 5D, titration of increasing concentrations of BAR-PH induced longer, more prominent bundles as examined by fluorescence microscopy, with maximum length achieved around 1 μM of BAR-PH. Low-speed co-sedimentation assays with increasing concentration of BAR-PH produced similar results.

We and others have previously observed that the stability of the BAR domain in some BAR domain-containing proteins requires the presence of its PH domain mate (Eberth et al., 2009; Nie et al., 2006), suggesting that the two domains fold together with integrated function. As the PH domain of ASAP1 binds to phosphatidylinositol 4,5-bisphosphate ($PI(4,5)P_2$), we tested if $PI(4,5)P_2$ affected the actin-bundling activity of the BAR domain. We performed the fluorescence-based bundling assay as described previously, in the absence or presence of large unilamellar vesicles, containing 2.5% $PI(4,5)P_2$. As shown in Figure S4I, the presence of phospholipids did not produce an appreciable effect on bundle length. We also considered that the PH domain may affect the activity independent of phospholipid binding. As we were unsuccessful in purifying the isolated BAR domain as a recombinant protein, we assessed the effects of the BAR domain on actin filaments using a cellular assay, as was done for Figure 2. As shown in Figures S4D–S4H, overexpression of the BAR domain alone did not produce an effect on total F-actin content, did not lead to stress fiber reorganization, ordid not lead to changes in cell shape, compared with the BAR-PH. Thus the PH domain is required for BAR domain-mediated bundling, although by itself PZA (see Figure 5) or the isolated PH domain (data not shown) was not sufficient to induce bundling. Together these results indicate that BAR-PH of ASAP1 bundles actin, which may regulate actin stress fibers, cortical actin, and actin microspikes.

We next determined if the BAR-PH tandem of ASAP1 is incorporated into bundled actin. F-actin was incubated alone, with ASAP1 BAR-PH, or with α-actinin, spotted on poly-L-lysine-coated coverslips, double-stained with mouse anti-His_6 antibody, followed by anti-mouse Alexa Fluor 594 and Phalloidin Alexa Fluor 488 and imaged by confocal microscopy. Single z-slices in Figure 5E indicate actin bundle formation in the presence of α-actinin (upper panel, F-actin), although there was no signal in the His_6 channel, as α-actinin

has no polyhistidine tag. In the representative slice from BAR-PH/F-actin IF, actin bundle formation is observed (upper panel, F-actin), with punctate signals from anti-His_6 staining decorating the bundles (lower panel, His_6), indicating incorporation of ASAP1 into the bundles at discrete intervals.

Interaction of actin-binding proteins with actin filaments may be driven by interactions between specific amino acid patches or may be electrostatically driven. If electrostatic, the strength of interaction with actin may depend on the ionic strength (Disanza et al., 2006; Mattila et al., 2007; Lee et al., 2007; Millard et al., 2007; Drager et al., 2017). Therefore, we performed the bundling assay between ASAP1 BAR-PH and F-actin at a 50–150 mM range of KCl concentration. As shown in Figure S4J, full actin-bundling activity of BAR-PH is retained at KCl concentration of 150 mM, suggesting that the binding is not based on purely electrostatic interactions.

The BAR-PH Tandem of a Related Arf GAP, ACAP1, Does Not Affect Actin Stress Fibers

In the human ArfGAP family, ACAPs and ASAPs are the only two subtypes that contain a BAR domain, with each subtype containing three members each (ASAP1–3 and ACAP1–3). To investigate whether the actin-modulating activity of BAR-PH is unique to ASAP1 or is shared between the groups, we overexpressed BAR-PH, ΔBARPH, or full-length ASAP1 and ACAP1 in 3T3 and HFF-1 fibroblasts and compared their effects on cell morphology and actin remodeling. ACAP1 is known to induce membrane protrusions, which we have observed; however, we did not detect actin microspikes or thickening of actin stress fibers in ACAP1 BAR-PH-overexpressing cells (closed white arrowheads) (Figures 6A, 6C, and S5A). Cells overexpressing ACAP1 BAR-PH had cell area and shape similar to that of the empty vector (Figures 6D, S5C, and S5D). Likewise, full-length ACAP1 overexpression did not increase filamentous actin content, compared with the empty vector control (Figures 6B, 6E, and S5B). We then examined whether ACAP1 BAR-PH is able to rescue the loss of filamentous actin caused by ASAP1 knockdown. Overexpression of ACAP1 in siASAP1 cells (knockdown efficiency is shown in Figure 7B) did not lead to restoration of F-actin or reappearance of stress fibers (Figures 7A and S6A). Moreover, overexpression of ACAP1-ASAP1 chimera, where the BAR-PH region of ASAP1 is replaced with that of ACAP1 did not rescue the effects of ASAP1 loss (Figures 7A and 7C). These results indicate that only ASAP1 BAR domain remodels actin structures.

DISCUSSION

ASAP1 has been previously implicated in modulating the actin cytoskeleton through its regulation of FA complexes. Here we report that (1) downregulation of ASAP1 results in perturbation of F-actin content and diminishes stress fiber network, (2) ASAP1 directly interacts with actin filaments through its N-BAR domain, and (3) the BAR-PH module is sufficient for actin binding and cellular actin remodeling. The effects of ASAP1 on the actin cytoskeleton may contribute, at least in part, to the reported effects of ASAP1 on differentiation, proliferation, invasion, and metastasis (Izdebska et al., 2018; Yang and Lin, 2018; Fife et al., 2014).

Regulation of actin is specific for a subset of BAR-domain-containing proteins. Several members of the N-BAR domain subfamily have been reported to directly bind to actin filaments—BIN1, PICK1, and, as described in this study, ASAP1 (Rocca et al., 2008; Drager et al., 2017), whereas two members, endophilin and oligophrenin-1, have been found to not directly interact with actin through their BAR domains (Kostan et al., 2014; Fauchereau et al., 2003). To evaluate if actin-remodeling properties are conserved within the BAR-containing group of the ArfGAP family, we compared the effect of the overexpression of ACAP1 and ASAP1 on actin in cultured cells. Although both are N-BAR-domain containing ArfGAPs, ACAP1 did not exert the same effect on the actin structures as ASAP1. Expression of the ACAP1-ASAP1 chimera, where the localization signal through the PXXP/SH3 domains is preserved, but the BAR-PH of ASAP1 is replaced with that of ACAP1, did not produce the same cellular effect as the full-length ASAP1. These results support the idea that, among the Arf GAPs, this mechanism for regulating actin is specific for the ASAP subtype, and the difference between the ASAP1 and ACAP1 BAR-PH domains is another example of disparate functions of BAR domains (Millard et al., 2007; Krugmann et al., 2001; Scita et al., 2008; Stanishneva-Konovalova et al., 2016; Kessels and Qualmann, 2015). In our ongoing studies, we are investigating structural determinants of interaction of the BAR domains with F-actin and whether this mechanism for regulating actin is preserved in the entire ASAP subfamily.

Actin-binding activity of ASAP1 BAR-PH is inhibited by the ArfGAP domain. In this study we observed that the presence of the ArfGAP domain reduces binding and bundling activity of BAR-PH and leads to a less

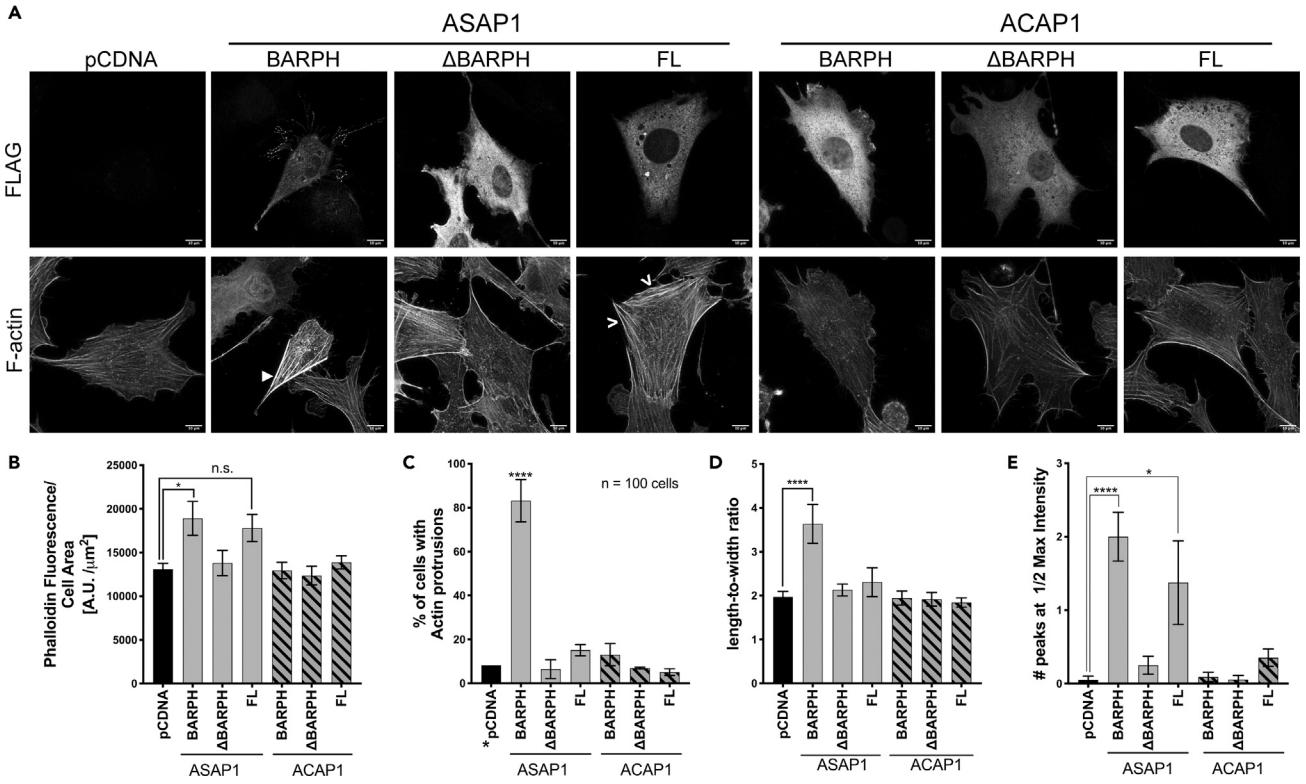

Figure 6. The ASAP1, but Not ACAP1, BAR-PH Tandem Induces Actin Remodeling and Leads to Cell Area Collapse

NIH 3T3 fibroblasts were transiently transfected with empty vector pCDNA or tagged BAR-PH, ΔBARPH, or full-length ACAP1 and ASAP1. Cells were processed as in Figure 2.

(A) Representative images of transfected cells. MIPs of representative transfected cells stained for FLAG or hemagglutinin tag (upper panel) and F-actin (phalloidin) (bottom panel) are shown. Closed white arrowhead indicates thickening of cortical actin induced by ASAP1 BAR-PH expression; open white arrowheads indicate increased intensity of F-actin staining induced by full-length ASAP1. Scale bar, 10 μm.

(B) Effect of ASAP1 and ACAP1 on F-actin content. F-actin content was estimated from quantification of fluorescence from phalloidin Alexa Fluor 488 as described in Figure 1. The mean ± SEM of total fluorescence (arbitrary units) divided by cell area is presented. See also Figure S5.

(C) Relative effects of ASAP1 and ACAP1 overexpression on the formation of microspikes. The average percentage, mean ± SEM, of cells expressing the indicated proteins that formed microspikes, labeled actin protrusions in the figure axis, is presented. As a control, random empty vector cells (labeled pCDNA in the figure) were counted.

(D) Relative effect of ASAP1 and ACAP1 on cell shape. The length-to-width ratios of cells expressing the indicated proteins were determined, the mean ± SEM is presented.

(E) Relative effect of ASAP1 and ACAP1 on stress fibers. In cells expressing the indicated proteins and labeled with phalloidin Alexa Fluor 488, two lines per cell were drawn perpendicular to the visualized stress fibers. The fluorescence intensity through the line was determined and the number of peaks with intensity greater than half of the maximum intensity peak was determined for 15 cells under each condition. The results are presented as the mean ± SEM. For (B, D, and E), n = 15 cells. *$p < 0.05$, ****$p < 0.0001$, n.s., not significant, compared with the empty vector control, one-way ANOVA with Tukey's post hoc tests. Results shown are a representative of at least three independent experiments and are independent of the transfection reagent used.

pronounced effect on cellular actin. We have previously reported that the BAR domain decreases the catalytic power of the ArfGAP domain toward its GTPase substrate, and a similar observation was made for other BAR domain-containing GAPs, such as RhoGAPs oligophrenin-1, and GRAF1 (Fauchereau et al., 2003; Jian et al., 2009; Eberth et al., 2009). This may suggest a reciprocal inter-domain regulation that coordinates spatiotemporal interaction of the ASAP1 GAP domain with Arf and of the N-BAR domain with actin, NM2A, or the membrane. In our future studies, we will examine how binding of ASAP1 substrates Arf1 and Arf5 contributes to the activity of the BAR domain of ASAP1.

Activity of the BAR domain of ASAP1 may also be regulated via C-terminal auto-inhibition. We observed that the fragments with intact SH3 domain inhibited formation of the actin microspikes and weakened actin binding, suggesting an auto-inhibitory role. Regulation of the BAR domains by their C termini is well documented. I-BAR domain member IRSp53 requires interactions of Esp8, WAVE1 and Mena, and Cdc42 to

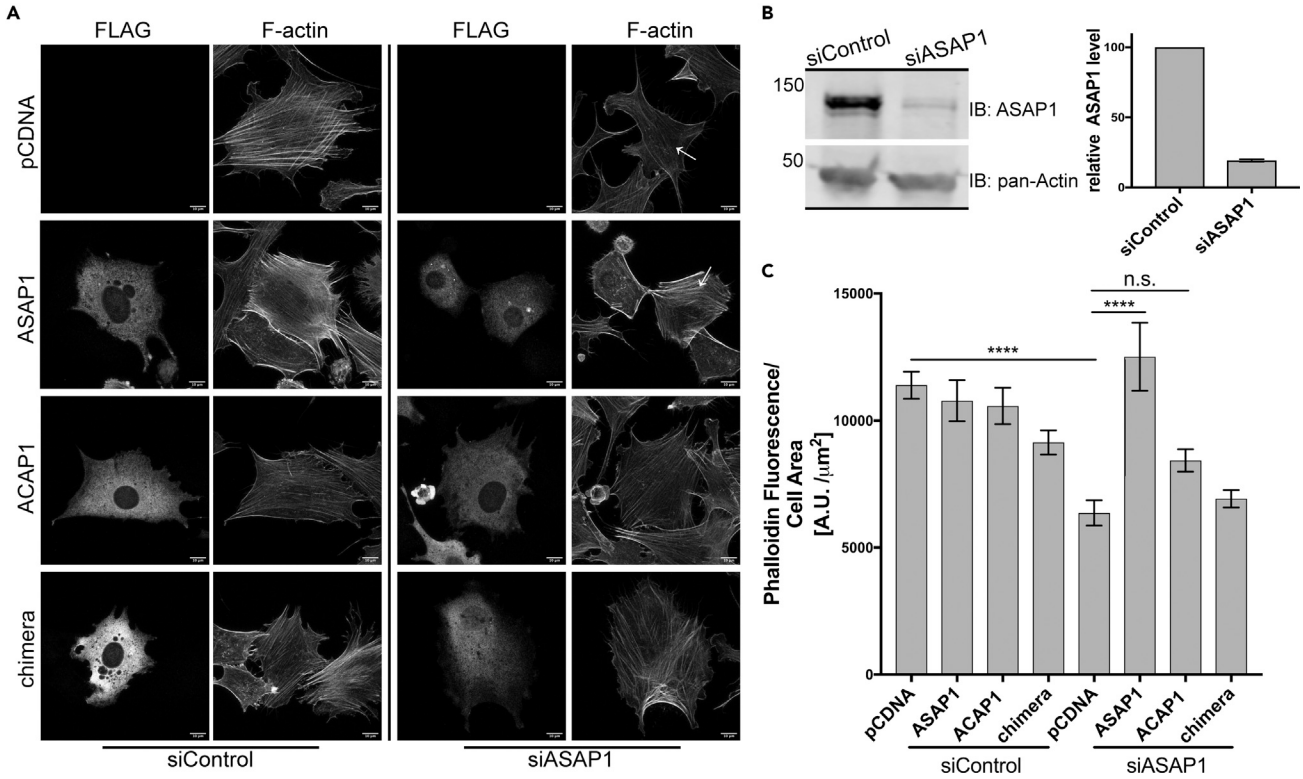

Figure 7. ACAP1 Is Unable to Restore Filamentous Actin Depletion Caused by ASAP1 Loss

NIH 3T3 cells were transfected with a control siRNA or siRNA against 3′ UTR region of mouse ASAP1. After 48 h, siControl and siASAP1 cells were transfected with empty vector (pCDNA), full-length ASAP1, ACAP1 or a chimera of the BAR-PH of ACAP1, and the ArfGAP, Ank repeat, proline-rich, E/DLPPKP, and SH3 domains of ASAP1; 24 h post-transfection (72 h total), cells were re-plated on fibronectin-coated coverslips and processed for imaging as before.

(A) Representative images of cells transfected with siRNA and expression plasmids as indicated. White arrows indicate loss of stress fibers in the cell body induced by ASAP1 knockdown (siASAP1 pCDNA) and the rescue of stress fibers following reconstitution of ASAP1 (siASAP1 ASAP1). See also Figure S6.

(B) Relative ASAP1 expression levels in the control and knockdown cells used for rescue. Protein levels were determined by immunoblot of cell lysates.

(C) Relative F-actin content of transfected cells. F-actin content was quantified as described in Figure 1. Data are mean ± SEM of a representative experiment, n = 15 cells, scale bar, 10 μm. ****p < 0.0001, n.s., not significant, one-way ANOVA with Tukey's post hoc tests, no significance was found in any other groups.

induce bundling activity and filopodia formation and SH3 domain serves both as an auto-inhibitory module and a localization signal (Misra et al., 2010, 2012; Disanza et al., 2006; Krugmann et al., 2001; Miki et al., 2000; Nakagawa, 2003; Yamagishi et al., 2004; Robens et al., 2010). F-BAR domain member syndapin I (PACSIN1), which contains an SH3 domain, connected by a long linker, is also subject to auto-regulation. The solved crystal structure of auto-inhibited syndapin I shows that the linker acts as a flexible arm allowing the SH3 domain to associate with F-BAR domain (Rao et al., 2010). Interaction of syndapin I SH3 domain with dynamin and WASL (Wiskott-Aldrich syndrome like) family of proteins might release auto-inhibition at sites of membrane remodeling (Roos and Kelly, 1998; Qualmann et al., 1999; Itoh et al., 2005). N-BAR domain member endophilin is also auto-inhibited by its SH3 domain, and interaction with dynamin through its proline-rich domain is required for recruitment of endophilin to the membrane (Meinecke et al., 2013). The C-terminal SH3 domain of ASAP1 connects to the GAP domain and ankyrin motifs through the proline-rich sequences and a stretch of E/DLPPKP repeats of unknown function and structure. This stretch is predicted to be intrinsically disordered and may be a flexible linker arm similar to that in syndapin I, allowing the SH3 domain to associate with the BAR domain. In preliminary experiments, we have found that the SH3 domain of ASAP1 binds to the BAR domain *in trans*, and future studies are aimed to determine the effect of SH3 on BAR domain-mediated actin bundling and whether SH3 binding partners can regulate the interaction.

In summary, we have tested the hypothesis that ASAP1 ArfGAP directly binds and bundles actin filaments through its N-BAR domain to control the organization of actin stress fibers. Our results indicate that ASAP1

controls cellular levels of filamentous actin, the BAR domain of ASAP1 participates in maintenance and arrangement of VSFs in fibroblasts, and the actin remodeling activity of ASAP1 is modulated by its GAP and SH3 domains. In our future studies, we will address the molecular basis of regulation of ASAP1 actin remodeling activity and the mechanism by which the GAP and the SH3 domains regulate actin bundling mediated by the ASAP1 BAR-PH.

Limitations of the Study

Our *in vitro* experimental evidence suggests that actin remodeling activity of ASAP1 is auto-inhibited intramolecularly by its C terminus. However, at present, we lack information on the mechanism of this regulation. Further investigation is required into the possible roles that binding partners of ASAP1 may play in controlling its actin remodeling activity. In addition, it is unknown how ASAP1 actin-reorganizing activity contributes to physiological processes, in which ASAP1 is a player, e.g., cell differentiation.

METHODS

All methods can be found in the accompanying Transparent Methods supplemental file.

SUPPLEMENTAL INFORMATION

Supplemental Information can be found online at https://doi.org/10.1016/j.isci.2019.11.015.

ACKNOWLEDGMENTS

We would like to thank Itoro Akpan and Dr. Valarie Barr (National Cancer Institute, Bethesda, MD) for technical assistance with confocal microscopy. We would like to thank Dr. James R. Sellers (National Heart, Lung, and Blood Institute, Bethesda, MD) for providing pre-formed actin filaments and for critical reading of the manuscript. We would also like to thank Dr. Vincent Schram and Lynne Holtzclaw (National Institute of Child Health and Human Development, Bethesda, MD) for feedback on sample preparation and microscopy image analysis. This work was supported by the Intramural Research Program of the National Cancer Institute, National Institutes of Health, Department of Health and Human Services (project number BC007365).

AUTHOR CONTRIBUTIONS

Conceptualization, P.A.R., A.G., and T.V.; Methodology, A.G., T.V., and P.A.R.; Validation, A.G. and T.V.; Investigation, Figures 1A–1G, 2, 3, 5, 6, 7, and S1–S6—A.G., Figures 1H–1I and 4, T.V.; Formal analysis, A.G. and T.V.; Resources, A.G., X.J., and R.L., Visualization, A.G.; Writing – Original Draft, A.G.; Writing – Review and Editing, A.G., T.V., R.L., X.J., and P.A.R., Funding Acquisition, P.A.R.; Supervision, P.A.R.

DECLARATION OF INTERESTS

The authors declare no competing interests.

Received: June 19, 2019
Revised: September 30, 2019
Accepted: November 6, 2019
Published: December 20, 2019

REFERENCES

Bharti, S., Inoue, H., Bharti, K., Hirsch, D.S., Nie, Z., Yoon, H.Y., Artym, V., Yamada, K.M., Mueller, S.C., Barr, V.A., and Randazzo, P.A. (2007). Src-dependent phosphorylation of ASAP1 regulates podosomes. Mol. Cell Biol. *27*, 8271–8283.

Blanchoin, L., Boujemaa-Paterski, R., Sykes, C., and Plastino, J. (2014). Actin dynamics, architecture, and mechanics in cell motility. Physiol. Rev. *94*, 235–263.

Brown, M.T., Andrade, J., Radhakrishna, H., Donaldson, J.G., Cooper, J.A., and Randazzo, P.A. (1998). ASAP1, a phospholipid-dependent arf GTPase-activating protein that associates with and is phosphorylated by Src. Mol. Cell Biol. *18*, 7038–7051.

Calafate, S., Flavin, W., Verstreken, P., and Moechars, D. (2016). Loss of Bin1 promotes the propagation of tau pathology. Cell Rep. *17*, 931–940.

Carman, P.J., and Dominguez, R. (2018). BAR domain proteins-a linkage between cellular membranes, signaling pathways, and the actin cytoskeleton. Biophys. Rev. *10*, 1587–1604.

Chen, P.W., Jian, X., Heissler, S.M., Le, K., Luo, R., Jenkins, L.M., Nagy, A., Moss, J., Sellers, J.R., and Randazzo, P.A. (2016). The arf GTPase-activating protein, ASAP1, binds nonmuscle myosin 2A to control remodeling of the actomyosin network. J. Biol. Chem. *291*, 7517–7526.

Disanza, A., Mantoani, S., Hertzog, M., Gerboth, S., Frittoli, E., Steffen, A., Berhoerster, K., Kreienkamp, H.-J., Milanesi, F., Fiore, P.P.D., et al. (2006). Regulation of cell shape by Cdc42 is mediated by the synergic actin-bundling activity of the Eps8–IRSp53 complex. Nat. Cell Biol. *8*, 1337–1347.

Dorland, Y.L., Malinova, T.S., Van Stalborch, A.M., Grieve, A.G., Van Geemen, D., Jansen, N.S., De Kreuk, B.J., Nawaz, K., et al. (2016). The F-BAR protein pacsin2 inhibits asymmetric VE-cadherin internalization from tensile adherens junctions. Nat. Commun. *7*, 12210.

Drager, N.M., Nachman, E., Winterhoff, M., Bruhmann, S., Shah, P., Katsinelos, T., Boulant, S., Teleman, A.A., Faix, J., and Jahn, T.R. (2017). Bin1 directly remodels actin dynamics through its BAR domain. EMBO Rep. *18*, 2051–2066.

Eberth, A., Lundmark, R., Gremer, L., Dvorsky, R., Koessmeier, K.T., Mcmahon, H.T., and Ahmadian, M.R. (2009). A BAR domain-mediated autoinhibitory mechanism for RhoGAPs of the GRAF family. Biochem. J. *417*, 371–377.

Ehlers, J.P., Worley, L., Onken, M.D., and Harbour, J.W. (2005). DDEF1 is located in an amplified region of chromosome 8q and is overexpressed in uveal melanoma. Clin. Cancer Res. *11*, 3609–3613.

Eltzner, B., Wollnik, C., Gottschlich, C., Huckemann, S., and Rehfeldt, F. (2015). The filament sensor for near real-time detection of cytoskeletal fiber structures. PLoS One *10*, e0126346.

Fauchereau, F., Herbrand, U., Chafey, P., Eberth, A., Koulakoff, A., Vinet, M.-C., Ahmadian, M.R., Chelly, J., and Billuart, P. (2003). The RhoGAP activity of OPHN1, a new F-actin-binding protein, is negatively controlled by its amino-terminal domain. Mol. Cell Neurosci. *23*, 574–586.

Fievez, S., and Carlier, M.F. (1993). Conformational changes in subdomain-2 of G-actin upon polymerization into F-actin and upon binding myosin subfragment-1. FEBS Lett. *316*, 186–190.

Fife, C.M., Mccarroll, J.A., and Kavallaris, M. (2014). Movers and shakers: cell cytoskeleton in cancer metastasis. Br. J. Pharmacol. *171*, 5507–5523.

Gavin, R.H. (1999). Synergy of cytoskeleton components - cytoskeletal polymers exhibit both structural and functional synergy. Bioscience *49*, 641–655.

Hotulainen, P., and Lappalainen, P. (2006). Stress fibers are generated by two distinct actin assembly mechanisms in motile cells. J. Cell Biol. *173*, 383–394.

Inoue, H., Ha, V.L., Prekeris, R., and Randazzo, P.A. (2008). Arf GTPase-activating protein ASAP1 interacts with Rab11 effector FIP3 and regulates pericentrosomal localization of transferrin receptor-positive recycling endosome. Mol. Biol. Cell *19*, 4224–4237.

Itoh, T., Erdmann, K.S., Roux, A., Habermann, B., Werner, H., and De Camilli, P. (2005). Dynamin and the actin cytoskeleton cooperatively regulate plasma membrane invagination by BAR and F-bar proteins. Dev. Cell *9*, 791–804.

Izdebska, M., Zielinska, W., Grzanka, D., and Gagat, M. (2018). The role of actin dynamics and actin-binding proteins expression in epithelial-to-mesenchymal transition and its association with cancer progression and evaluation of possible therapeutic targets. Biomed. Res. Int. *2018*, 4578373.

Jian, X., Brown, P., Schuck, P., Gruschus, J.M., Balbo, A., Hinshaw, J.E., and Randazzo, P.A. (2009). Autoinhibition of Arf GTPase-activating protein activity by the BAR domain in ASAP1. J. Biol. Chem. *284*, 1652–1663.

Kahn, R.A., Bruford, E., Inoue, H., Logsdon, J.M., Jr., Nie, Z., Premont, R.T., Randazzo, P.A., Satake, M., Theibert, A.B., Zapp, M.L., and Cassel, D. (2008). Consensus nomenclature for the human ArfGAP domain-containing proteins. J. Cell Biol. *182*, 1039–1044.

Katoh, K., Kano, Y., and Fujiwara, K. (2000). Isolation and in vitro contraction of stress fibers. Methods Enzymol. *325*, 369–380.

Kessels, M.M., and Qualmann, B. (2015). Different functional modes of BAR domain proteins in formation and plasticity of mammalian postsynapses. J. Cell Sci. *128*, 3177–3185.

King, F.J., Hu, E., Harris, D.F., Sarraf, P., Spiegelman, B.M., and Roberts, T.M. (1999). DEF-1, a novel Src SH3 binding protein that promotes adipogenesis in fibroblastic cell lines. Mol. Cell Biol. *19*, 2330–2337.

Kostan, J., Salzer, U., Orlova, A., Toro, I., Hodnik, V., Senju, Y., Zou, J., Schreiner, C., Steiner, J., Merilainen, J., et al. (2014). Direct interaction of actin filaments with F-BAR protein pacsin2. EMBO Rep. *15*, 1154–1162.

Kovac, B., Teo, J.L., Makela, T.P., and Vallenius, T. (2013). Assembly of non-contractile dorsal stress fibers requires alpha-actinin-1 and Rac1 in migrating and spreading cells. J. Cell Sci. *126*, 263–273.

Krugmann, S., Jordens, I., Gevaert, K., Driessens, M., Vandekerckhove, J., and Hall, A. (2001). Cdc42 induces filopodia by promoting the formation of an IRSp53:Mena complex. Curr. Biol. *11*, 1645–1655.

Lappalainen, P. (2016). Actin-binding proteins: the long road to understanding the dynamic landscape of cellular actin networks. Mol. Biol. Cell *27*, 2519–2522.

Lasorsa, A., Malki, I., Cantrelle, F.X., Merzougui, H., Boll, E., Lambert, J.C., and Landrieu, I. (2018). Structural basis of tau interaction with BIN1 and regulation by tau phosphorylation. Front. Mol. Neurosci. *11*, 421.

Lee, S.H., Kerff, F., Chereau, D., Ferron, F., Klug, A., and Dominguez, R. (2007). Structural basis for the actin-binding function of missing-in-metastasis. Structure *15*, 145–155.

Li, H., Zhang, D., Yu, J., Liu, H., Chen, Z., Zhong, H., and Wan, Y. (2018). CCL18-dependent translocation of AMAP1 is critical for epithelial to mesenchymal transition in breast cancer. J. Cell Physiol. *233*, 3207–3217.

Lin, D., Watahiki, A., Bayani, J., Zhang, F., Liu, L., Ling, V., Sadar, M.D., English, J., Fazli, L., So, A., et al. (2008). ASAP1, a gene at 8q24, is associated with prostate cancer metastasis. Cancer Res. *68*, 4352–4359.

Lin-Jones, J., and Burnside, B. (2007). Retina-specific protein fascin 2 is an actin cross-linker associated with actin bundles in photoreceptor inner segments and calycal processes. Invest. Ophthalmol. Vis. Sci. *48*, 1380–1388.

Liu, Y., Loijens, J.C., Martin, K.H., Karginov, A.V., and Parsons, J.T. (2002). The association of ASAP1, an ADP ribosylation factor-GTPase activating protein, with focal adhesion kinase contributes to the process of focal adhesion assembly. Mol. Biol. Cell *13*, 2147–2156.

Liu, Y., Yerushalmi, G.M., Grigera, P.R., and Parsons, J.T. (2005). Mislocalization or reduced expression of Arf GTPase-activating protein ASAP1 inhibits cell spreading and migration by influencing Arf1 GTPase cycling. J. Biol. Chem. *280*, 8884–8892.

Mattila, P.K., Pykalainen, A., Saarikangas, J., Paavilainen, V.O., Vihinen, H., Jokitalo, E., and Lappalainen, P. (2007). Missing-in-metastasis and IRSp53 deform PI(4,5)P2-rich membranes by an inverse BAR domain-like mechanism. J. Cell Biol. *176*, 953–964.

Mazelova, J., Astuto-Gribble, L., Inoue, H., Tam, B.M., Schonteich, E., Prekeris, R., Moritz, O.L., Randazzo, P.A., and Deretic, D. (2009). Ciliary targeting motif VxPx directs assembly of a trafficking module through Arf4. EMBO J. *28*, 183–192.

Meinecke, M., Boucrot, E., Camdere, G., Hon, W.C., Mittal, R., and Mcmahon, H.T. (2013). Cooperative recruitment of dynamin and BIN/amphiphysin/Rvs (BAR) domain-containing proteins leads to GTP-dependent membrane scission. J. Biol. Chem. *288*, 6651–6661.

Miki, H., Yamaguchi, H., Suetsugu, S., and Takenawa, T. (2000). IRSp53 is an essential intermediate between Rac and WAVE in the regulation of membrane ruffling. Nature *408*, 732–735.

Millard, T.H., Bompard, G., Heung, M.Y., Dafforn, T.R., Scott, D.J., Machesky, L.M., and Fütterer, K. (2005). Structural basis of filopodia formation induced by the IRSp53/MIM homology domain of human IRSp53. EMBO J. *24*, 240–250.

Millard, T.H., Dawson, J., and Machesky, L.M. (2007). Characterisation of IRTKS, a novel IRSp53/MIM family actin regulator with distinct filament bundling properties. J. Cell Sci. *120*, 1663–1672.

Misra, A., George, B., Rajmohan, R., Jain, N., Wong, M.H., Kambadur, R., and Thanabalu, T. (2012). Insulin Receptor Substrate protein 53kDa (IRSp53) is a negative regulator of myogenic differentiation. Int. J. Biochem. Cell Biol. *44*, 928–941.

Misra, A., Rajmohan, R., Lim, R.P.Z., Bhattacharyya, S., and Thanabalu, T. (2010). The mammalian Verprolin, WIRE induces filopodia independent of N-WASP through IRSp53. Exp. Cell Res. *316*, 2810–2824.

Muller, T., Stein, U., Poletti, A., Garzia, L., Rothley, M., Plaumann, D., Thiele, W., Bauer, M., Galasso, A., Schlag, P., et al. (2010). ASAP1 promotes tumor cell motility and invasiveness, stimulates metastasis formation in vivo, and correlates with poor survival in colorectal cancer patients. Oncogene *29*, 2393–2403.

Nakagawa, H. (2003). IRSp53 is colocalised with WAVE2 at the tips of protruding lamellipodia and filopodia independently of Mena. J. Cell Sci. *116*, 2577–2583.

Nie, Z., Hirsch, D.S., Luo, R., Jian, X., Stauffer, S., Cremesti, A., Andrade, J., Lebowitz, J., Marino, M., Ahvazi, B., et al. (2006). A BAR domain in the N terminus of the Arf GAP ASAP1 affects membrane structure and trafficking of epidermal growth factor receptor. Curr. Biol. *16*, 130–139.

Oakes, P.W., Beckham, Y., Stricker, J., and Gardel, M.L. (2012). Tension is required but not sufficient for focal adhesion maturation without a stress fiber template. J. Cell Biol. *196*, 363–374.

Oda, A., Wada, I., Miura, K., Okawa, K., Kadoya, T., Kato, T., Nishihara, H., Maeda, M., Tanaka, S., Nagashima, K., et al. (2003). CrkL directs ASAP1 to peripheral focal adhesions. J. Biol. Chem. *278*, 6456–6460.

Onodera, Y., Hashimoto, S., Hashimoto, A., Morishige, M., Mazaki, Y., Yamada, A., Ogawa, E., Adachi, M., Sakurai, T., Manabe, T., et al. (2005). Expression of AMAP1, an ArfGAP, provides novel targets to inhibit breast cancer invasive activities. EMBO J. *24*, 963–973.

Pollard, T.D. (2016). Actin and actin-binding proteins. Cold Spring Harb. Perspect. Biol. *8*, a018226.

Qualmann, B., Roos, J., Digregorio, P.J., and Kelly, R.B. (1999). Syndapin I, a synaptic dynamin-binding protein that associates with the neural Wiskott-Aldrich syndrome protein. Mol. Biol. Cell *10*, 501–513.

Randazzo, P.A., Andrade, J., Miura, K., Brown, M.T., Long, Y.Q., Stauffer, S., Roller, P., and Cooper, J.A. (2000). The Arf GTPase-activating protein ASAP1 regulates the actin cytoskeleton. Proc. Natl. Acad. Sci. U S A *97*, 4011–4016.

Rao, Y., Ma, Q., Vahedi-Faridi, A., Sundborger, A., Pechstein, A., Puchkov, D., Luo, L., Shupliakov, O., Saenger, W., and Haucke, V. (2010). Molecular basis for SH3 domain regulation of F-BAR-mediated membrane deformation. Proc. Natl. Acad. Sci. U S A *107*, 8213–8218.

Robens, J.M., Yeow-Fong, L., Ng, E., Hall, C., and Manser, E. (2010). Regulation of IRSp53-dependent filopodial dynamics by antagonism between 14-3-3 binding and SH3-mediated localization. Mol. Cell Biol. *30*, 829–844.

Rocca, D.L., Martin, S., Jenkins, E.L., and Hanley, J.G. (2008). Inhibition of Arp2/3-mediated actin polymerization by PICK1 regulates neuronal morphology and AMPA receptor endocytosis. Nat. Cell Biol. *10*, 259–271.

Roos, J., and Kelly, R.B. (1998). Dap160, a neural-specific Eps15 homology and multiple SH3 domain-containing protein that interacts with Drosophila dynamin. J. Biol. Chem. *273*, 19108–19119.

Rougerie, P., Miskolci, V., and Cox, D. (2013). Generation of membrane structures during phagocytosis and chemotaxis of macrophages: role and regulation of the actin cytoskeleton. Immunol. Rev. *256*, 222–239.

Sato, H., Hatanaka, K.C., Hatanaka, Y., Hatakeyama, H., Hashimoto, A., Matsuno, Y., Fukuda, S., and Sabe, H. (2014). High level expression of AMAP1 protein correlates with poor prognosis and survival after surgery of head and neck squamous cell carcinoma patients. Cell Commun. Signal. *12*, 17.

Scita, G., Confalonieri, S., Lappalainen, P., and Suetsugu, S. (2008). IRSp53: crossing the road of membrane and actin dynamics in the formation of membrane protrusions. Trends Cell Biol. *18*, 52–60.

Stanishneva-Konovalova, T.B., Derkacheva, N.I., Polevova, S.V., and Sokolova, O.S. (2016). The role of BAR domain proteins in the regulation of membrane dynamics. Acta Nat. *8*, 60–69.

Tanna, C.E., Goss, L.B., Ludwig, C.G., and Chen, P.W. (2019). Arf GAPs as regulators of the actin cytoskeleton-an update. Int. J. Mol. Sci. *20*, E442.

Tojkander, S., Gateva, G., Husain, A., Krishnan, R., and Lappalainen, P. (2015). Generation of contractile actomyosin bundles depends on mechanosensitive actin filament assembly and disassembly. Elife *4*, e06126.

Tojkander, S., Gateva, G., and Lappalainen, P. (2012). Actin stress fibers–assembly, dynamics and biological roles. J. Cell Sci. *125*, 1855–1864.

Tojkander, S., Gateva, G., Schevzov, G., Hotulainen, P., Naumanen, P., Martin, C., Gunning, P.W., and Lappalainen, P. (2011). A molecular pathway for myosin II recruitment to stress fibers. Curr. Biol. *21*, 539–550.

Vallenius, T. (2013). Actin stress fibre subtypes in mesenchymal-migrating cells. Open Biol. *3*, 130001.

Vonna, L., Wiedemann, A., Aepfelbacher, M., and Sackmann, E. (2007). Micromechanics of filopodia mediated capture of pathogens by macrophages. Eur. Biophys. J. *36*, 145–151.

Wang, J., Morita, Y., Mazelova, J., and Deretic, D. (2012). The Arf GAP ASAP1 provides a platform to regulate Arf4- and Rab11-Rab8-mediated ciliary receptor targeting. EMBO J. *31*, 4057–4071.

Wang, Y.L. (1984). Reorganization of actin filament bundles in living fibroblasts. J. Cell Biol. *99*, 1478–1485.

Wynn, T.A., Chawla, A., and Pollard, J.W. (2013). Macrophage biology in development, homeostasis and disease. Nature *496*, 445–455.

Yamada, H., Abe, T., Satoh, A., Okazaki, N., Tago, S., Kobayashi, K., Yoshida, Y., Oda, Y., Watanabe, M., Tomizawa, K., et al. (2013). Stabilization of actin bundles by a dynamin 1/cortactin ring complex is necessary for growth cone filopodia. J. Neurosci. *33*, 4514–4526.

Yamada, H., Takeda, T., Michiue, H., Abe, T., and Takei, K. (2016). Actin bundling by dynamin 2 and cortactin is implicated in cell migration by stabilizing filopodia in human non-small cell lung carcinoma cells. Int. J. Oncol. *49*, 877–886.

Yamagishi, A., Masuda, M., Ohki, T., Onishi, H., and Mochizuki, N. (2004). A novel actin bundling/filopodium-forming domain conserved in insulin receptor tyrosine kinase substrate p53 and missing in metastasis protein. J. Biol. Chem. *279*, 14929–14936.

Yang, X., and Lin, Y. (2018). Functions of nuclear actin-binding proteins in human cancer. Oncol. Lett. *15*, 2743–2748.

Yonenaga, Y., Mori, A., Onodera, H., Yasuda, S., Oe, H., Fujimoto, A., Tachibana, T., and Imamura, M. (2005). Absence of smooth muscle actin-positive pericyte coverage of tumor vessels correlates with hematogenous metastasis and prognosis of colorectal cancer patients. Oncology *69*, 159–166.

ISCI, Volume *22*

Supplemental Information

The ArfGAP ASAP1 Controls Actin Stress Fiber Organization via Its N-BAR Domain

Anjelika Gasilina, Teresa Vitali, Ruibai Luo, Xiaoying Jian, and Paul A. Randazzo

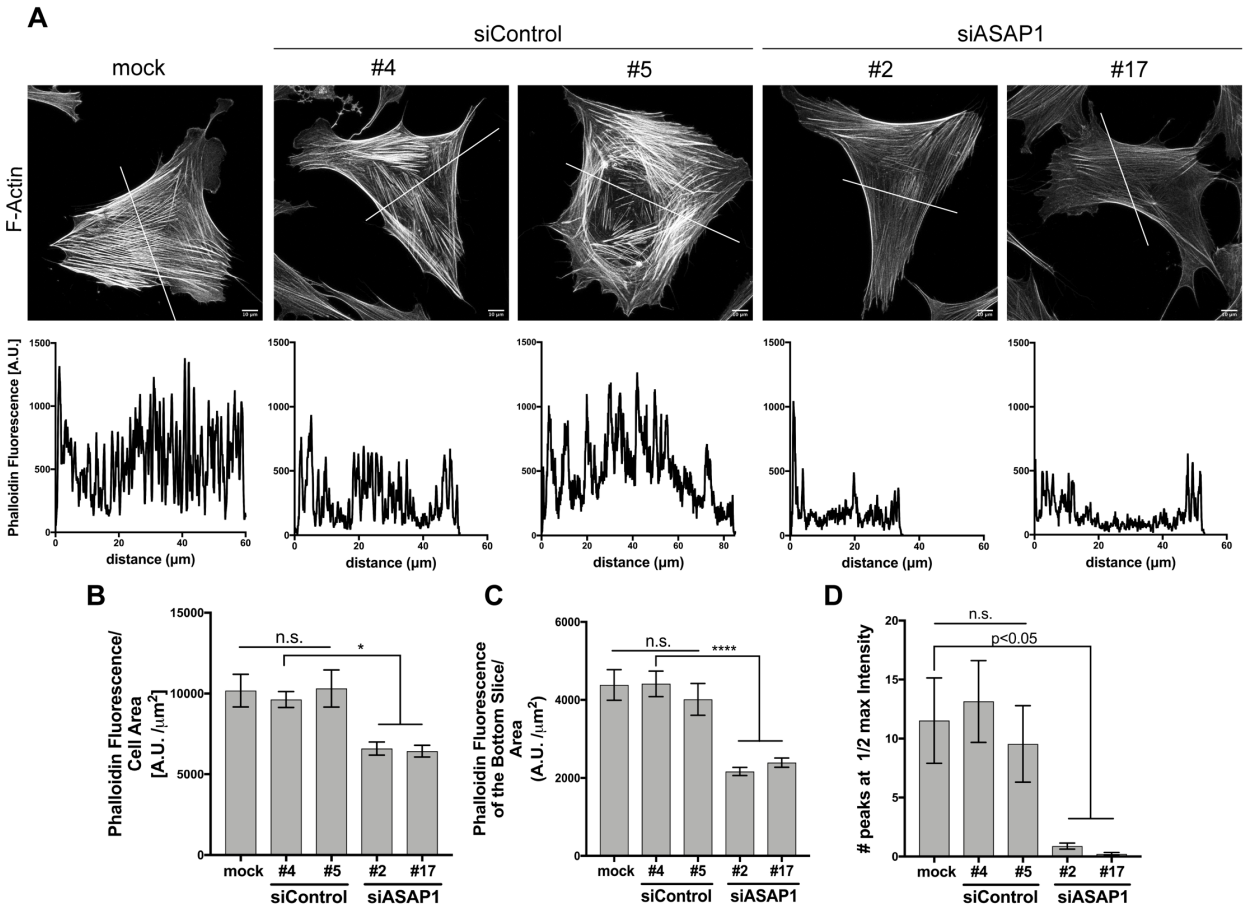

Figure S1. Reduced ASAP1 expression decreases levels of filamentous actin and affects distribution of stress fibers, Related to Figure 1.

A – D. Primary human foreskin fibroblasts (HFF-1) were mock treated or transiently transfected with two independent control or ASAP1 siRNAs. Post-transfection, cells were replated on fibronectin coated coverslips, fixed and stained with Phalloidin Alexa Fluor 488. **A**. Effect of reduced ASAP1 expression on actin distribution. Representative maximum intensity projection (MIP) images with a line scan profile below each image showing changes in intensity and distribution of fluorescence from Phalloidin Alexa Fluor 488 (white lines indicate approximately where scans were measured). **B**. Effect of reduced ASAP1 expression on cell F-actin content. Total Phalloidin Alexa Fluor 488 fluorescence as a readout for filamentous actin content of the whole cell was measured per cell area as described in Fig 1 and methods. **C**. As in **B**, but measured for the bottom cell slice only. **D**. Effect of reduced ASAP1 expression on stress fibers. Estimates of the number of stress fibers were calculated from analysis of line scans. Peaks with an intensity equal to or greater than the half maximal observed intensity were counted as stress fibers. 2 line scans were analyzed for each cell. See main figure for the immunoblot confirming the knockdown. Scale bar = 10 µm, n = 15 cells. *p<0.05, ****p < 0.0001, n.s. – not significant (one-way ANOVA) or p<0.05 (ANOVA on ranks). Data are mean ± s.e.m. of one of three representative experiments.

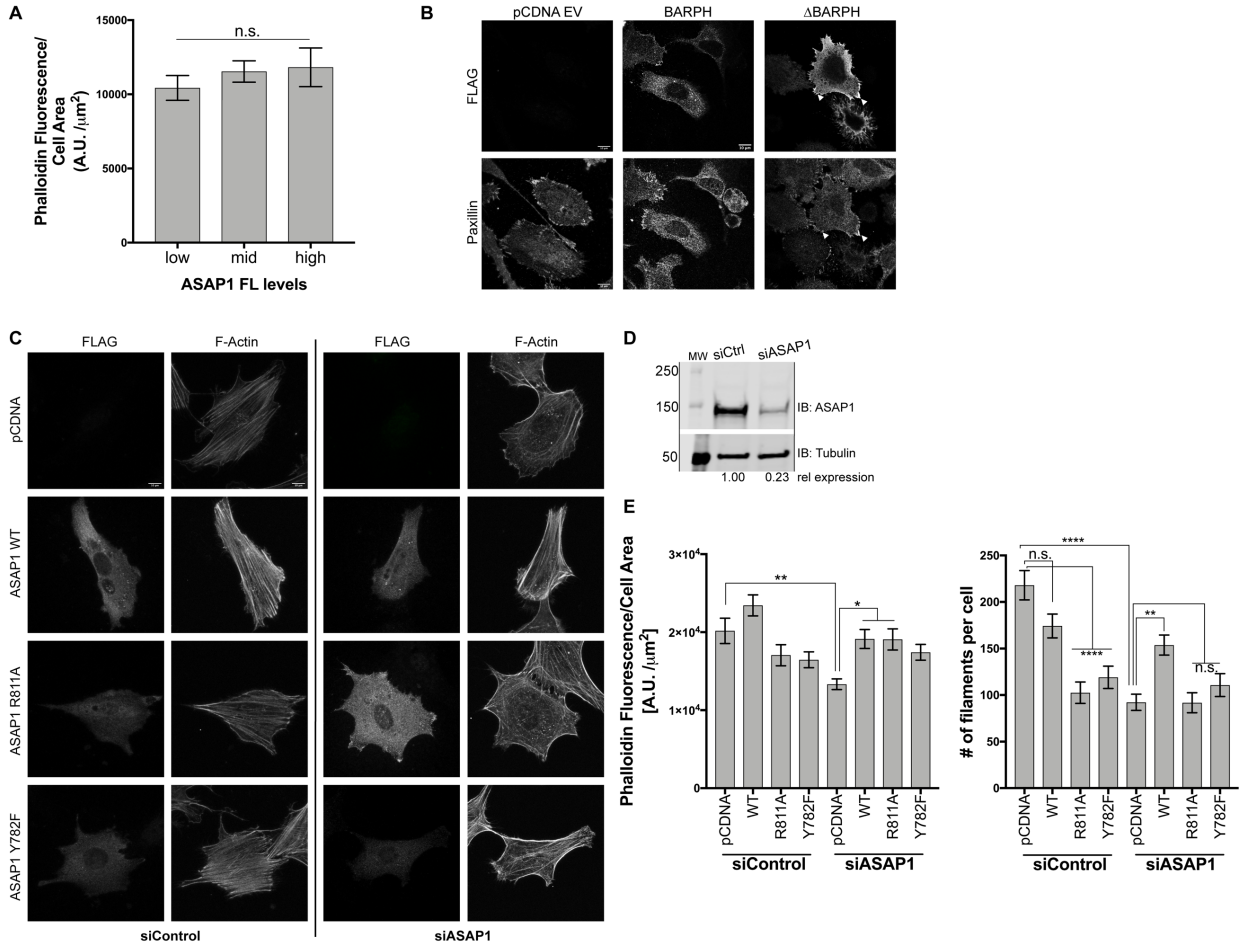

Figure S2, Data Related to Main Figure 2.

A. Lowest detectable levels of ectopic ASAP1 expression are sufficient to support F-actin levels in cells. Whole cell phalloidin fluorescence from main Fig. 2 (ASAP1 FL) was plotted according to the levels of ASAP1 expression as quantified by FLAG-staining. **B.** ASAP1 effect on actin remodeling can be separated from FA targeting. Human cervical carcinoma cells HeLa were transiently transfected with plasmids encoding empty vector (pCDNA EV), ASAP1 BARPH or ASAP1 ΔBARPH. After 24 hours cells were re-plated on fibronectin as before and stained with FLAG (epitope tag) and paxillin (focal adhesion marker) antibodies and processed for microscopy. Representative images of transfected cells indicate localization of the ΔBARPH mutant of ASAP1 to the immature adhesions (closed arrowheads). **C - E.** Part of ASAP1 effect on remodeling is dependent on Src/ CrkL binding and tyrosine phosphorylation. NIH/3T3 fibroblasts were transiently transfected with a control siRNA or siRNA against the 3'UTR region of human ASAP1. After 48 hours, siControl and siASAP1 cells were transfected with empty vector (pCDNA), or pCDNA with the open reading frame for full length ASAP1 WT, R811A (reduced Src binding) or Y782F (Src-phosphorylation site mutant). 24 hours later (72 hours total), cells were replated on fibronectin-coated coverslips and processed for confocal imaging as before. **C.** Representative images of the transfected cells. MIPs of cells stained for the epitope tag (FLAG) on the indicated protein and with Phalloidin Alexa Fluor 594 to visualize actin filaments in control and knockdown cells. **D.** Immunoblot confirming knockdown. **E.** (left panel) F-actin levels in transfected cells. Relative actin levels were estimated by quantifying total Phalloidin Alexa Fluor 594 fluorescence. The signal was normalized to cell area. A.U. is arbitrary fluorescence unit, (right panel) estimation of the number of filaments per cell in transfected cells. Results are presented as mean ± s.e.m. and are representative of two independent experiments, scale bar = 10 μm, n = 15 cells, n.s. = not significant, * $p<0.05$, ** $p<0.01$, **** $p<0.0001$, one-way ANOVA with Tukey's post hoc tests.

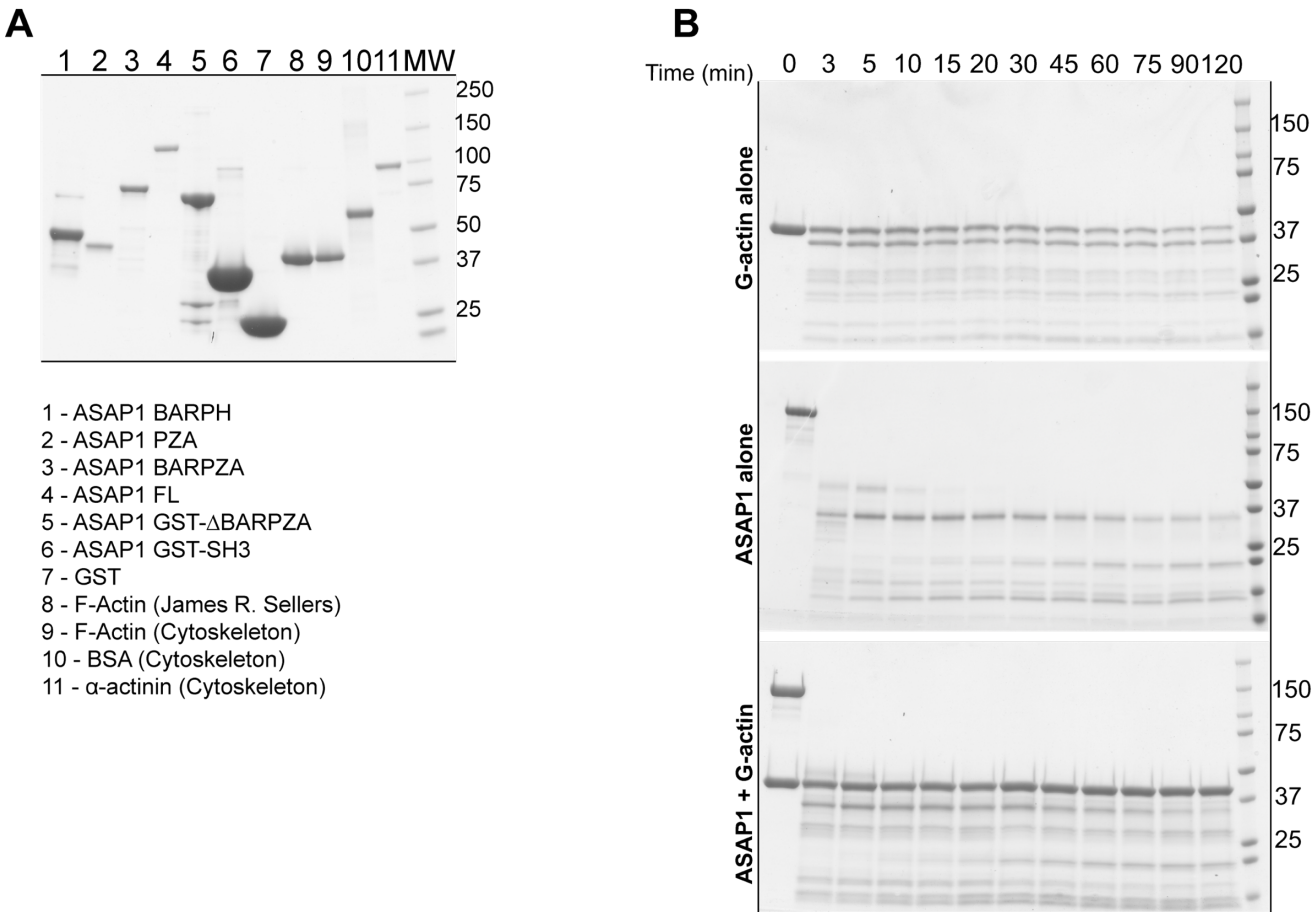

Figure S3. ASAP1 binds directly to actin filaments, Related to Figures 3, 4 and 5.
A. Purity of the proteins used for this study was assessed by SDS-PAGE (4 - 20% Bio-Rad), 1 – 7 were purified in the lab, 8 – provided by Dr. James R. Sellers, 9 – 11 are from commercial sources. **B.** ASAP1 is not protected by G-actin. The subtilisin A proteolysis protection assay was performed as a measure of protein-protein interaction. Subtilisin A (0.1 μg/ml) was incubated with ASAP1 (1 mg/mL) and G-actin (0.5 mg/mL), with ASAP1 alone (1 mg/mL) or G-actin alone (0.5 mg/mL) as indicated. Aliquots were taken at the indicated timepoints, resolved on a gradient (4-20%) SDS-PAGE and stained with GelCode Blue. Representative gels of proteolytic products of G-actin (top gel), ASAP1 (middle gel) and ASAP1 incubated with G-actin (bottom gel) are shown and are representative of at least 3 independent experiments.

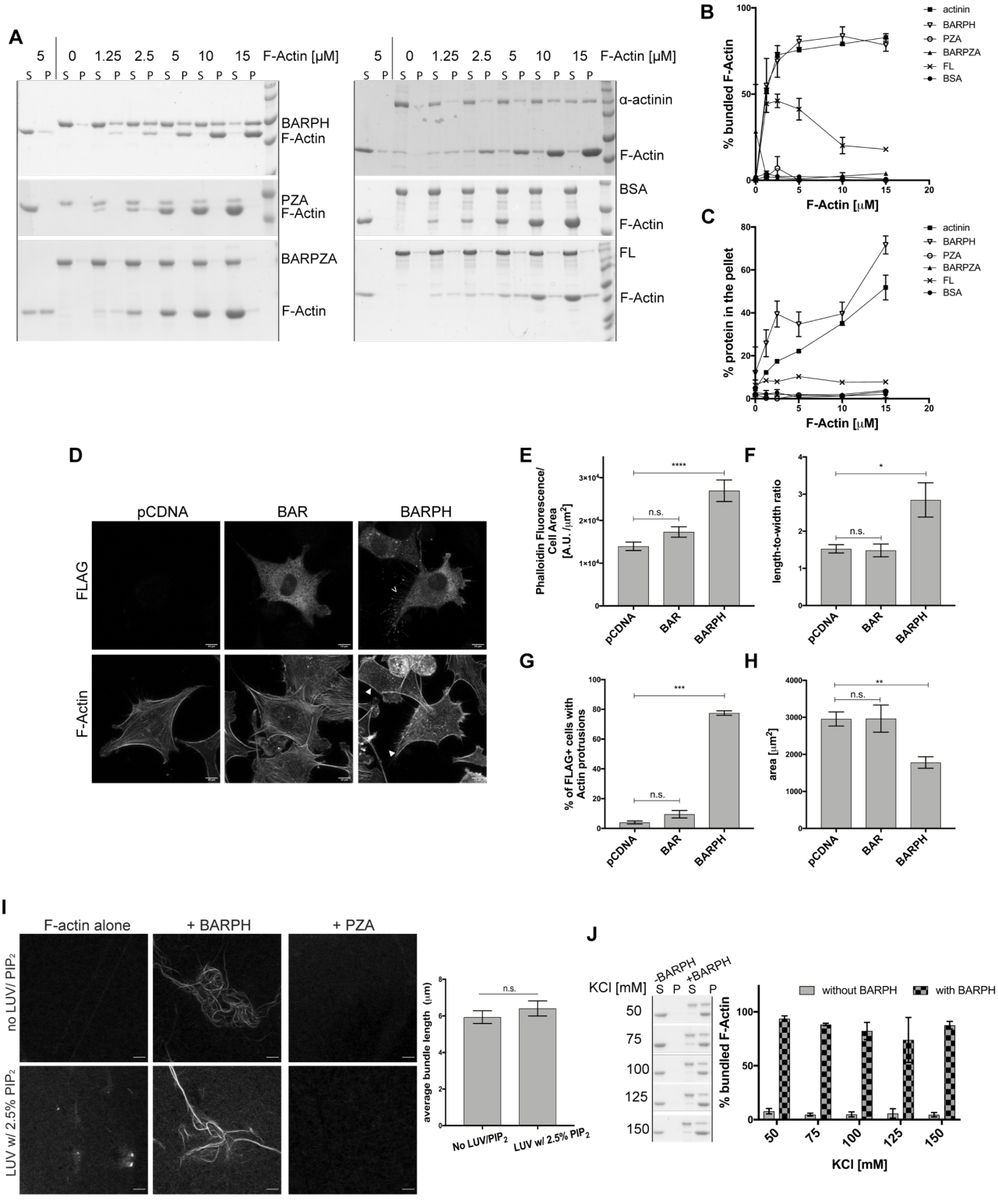
A
5 0 1.25 2.5 5 10 15 F-Actin [μM]
S P S P S P S P S P S P S P
BARPH
F-Actin
PZA
F-Actin
BARPZA
F-Actin
α-actinin
F-Actin
BSA
F-Actin
FL
F-Actin
B
% bundled F-Actin
F-Actin [μM]
actinin
BARPH
PZA
BARPZA
FL
BSA
C
% protein in the pellet
F-Actin [μM]
D
pCDNA
BAR
BARPH
FLAG
F-Actin
E
Phalloidin Fluorescence/ Cell Area [A.U./μm²]
n.s.
****
pCDNA
BAR
BARPH
F
length-to-width ratio
n.s.
*
G
% of FLAG+ cells with Actin protrusions
n.s.
***
H
area [μm²]
n.s.
**
I
F-actin alone
+ BARPH
+ PZA
no LUV/ PIP2
LUV w/ 2.5% PIP2
average bundle length (μm)
n.s.
No LUV/PIP2
LUV w/ 2.5% PIP2
J
KCl [mM]
-BARPH
+BARPH
S P S P
50
75
100
125
150
% bundled F-Actin
without BARPH
with BARPH
KCl [mM]

Figure S4. ASAP1 bundles actin filaments *in vitro* through its N-BAR domain and the C-terminus of ASAP1 negatively modulates the bundling activity, Related to Figure 5.

A – C. Actin bundling measured by low-speed actin co-sedimentation. **A.** F-actin alone (5 μM), ASAP1 full-length or truncations alone (2 μM) or in combination with increasing concentrations of F-Actin (as indicated) were incubated at room temperature for 30 min in F-buffer and subjected to sedimentation at 14,000 x g. α-actinin and BSA were used as positive and negative controls, respectively. Equal volumes of supernatant (S) and resuspended pellet (P) were resolved on single percentage (10% or 12%) SDS-PAGE and stained with GelCode Blue. Actin in the pellet was considered bundled actin. **B.** Actin concentration dependence of bundling induced by ASAP1. Gel images were analyzed in ImageStudio Lite (LI-COR) to determine the percentage of total actin than was in the precipitate (% bundles F-Actin). **C.** Actin concentration dependence of association of the indicated proteins with the bundled actin. The percentage of the indicated protein that coprecipitated with actin was calculated by analyzing the images as in **B. D – H.** BAR domain is inactive without PH domain. NIH/3T3 fibroblasts were transiently transfected with the empty vector (pCDNA) or vector encoding BAR or BAR-PH of ASAP1. Cells were processed as before. **D.** Representative images of the transfected cells. MIPs of cells stained for epitope tag (FLAG) and Phalloidin Alexa Fluor 488 to visualized F-actin. White open arrowheads indicate protrusions and white closed arrowheads indicate actin microspikes formed as a result of ASAP1 BAR-PH overexpression. Note no protrusions or actin remodeling induced by the BAR domain alone. **E.** Effect of BAR and BAR-PH on total cellular F-actin levels. Relative levels of F-actin were estimated by measuring total cell fluorescence of Phalloidin AF 488, with signal normalized to the cell area. **F.** Effect of BAR and BAR-PH on cell shape. The length-to-width ratio of cells was measured as described in Figure 2 as an indicator of cell shape. **G.** Effect of ASAP1 BAR and BAR-PH on actin protrusions. The percentage of FLAG-positive cells with actin protrusions is presented. Random empty vector cells were counted for presence of protrusions as the control. **H.** Effect of overexpression of BAR and BAR-PH on cell area. Cell area was determined as described for Figure 2. A representative experiment of three independent experiments is shown. **I.** Effect of lipid binding on the actin bundling activity of BARPH. Rabbit muscle F-actin (3 μM) alone or with ASAP1 BARPH or PZA (1 μM) was mixed in F-actin buffer in the absence or presence of large unilamellar vesicles (LUVs) containing 2.5% $PI(4,5)P_2$ and spotted on poly-L-lysine coated coverslips. Samples were processed as in main Figure 5. Average bundle length in two treatment groups was quantified using Ridge Detection plugin, as described in Methods. Results are representative of two different protein preparations and two different experiments, n.s. – not significant. **J.** Effect of ionic strength on actin bundling induced by ASAP1. F-Actin alone (5 μM) or with ASAP1 BAR-PH (2 μM) was incubated in F-actin buffer, containing indicated concentrations of KCl. Low-speed centrifugation was performed as in **A** and F-Actin in the pellet in the presence of BAR-PH (% bundled F-actin) was determined as described in **B.** The data for all experiments are summarized as means ± s.e.m., 15 cells per condition were analyzed for panels **E, F** and **H**, 100 cells per condition were analyzed for panel **G**. The data were analyzed with one-way ANOVA followed by multiple comparisons using the Tukey's post hoc test, scale bars = 10 μm, n.s. – not significant, ** = $p<0.01$, *** = $p<0.001$, **** = $p<0.0001$.

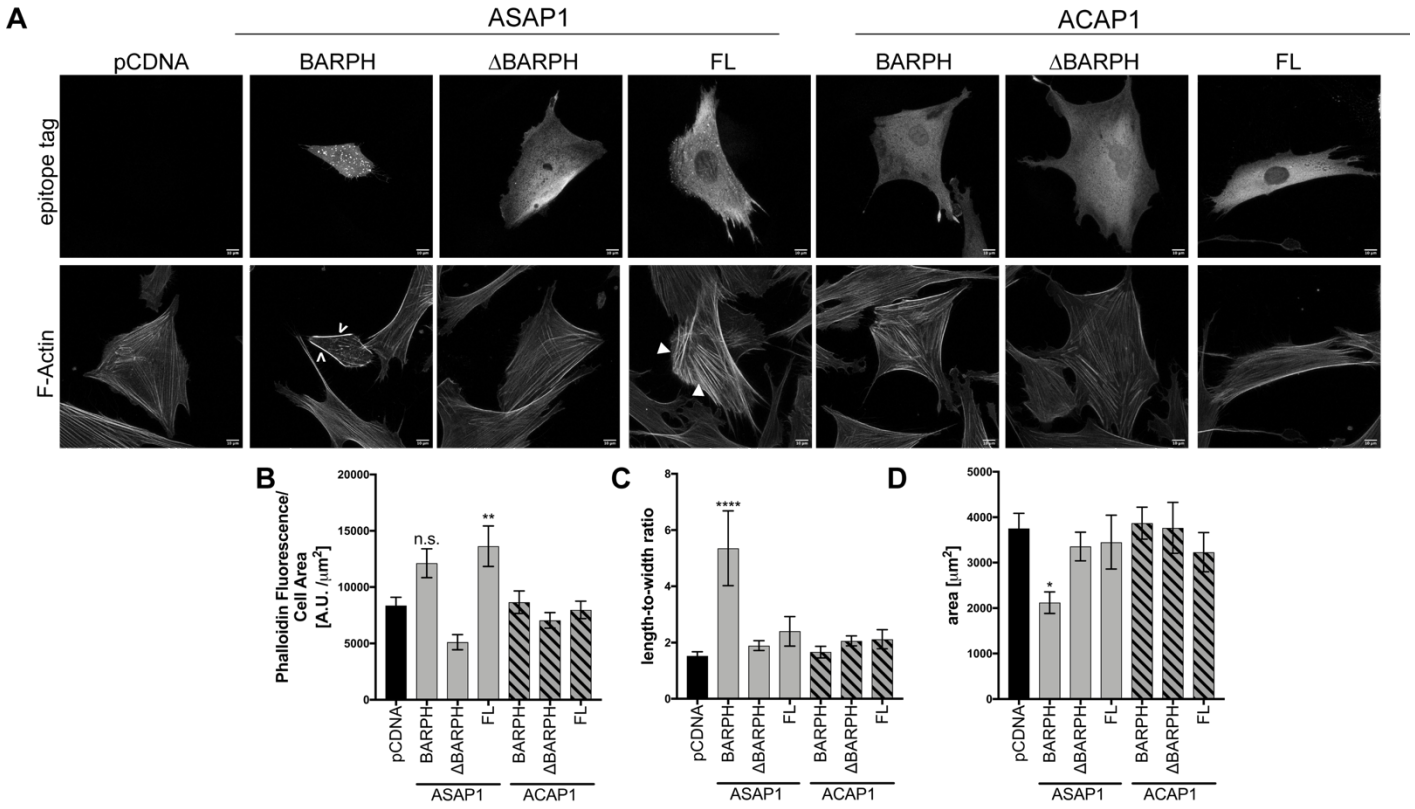

Figure S5. The ASAP1, but not the ACAP1, BAR-PH tandem induces actin remodeling and cell area collapse, Related to Figure 6.

Primary human foreskin fibroblasts (HFF-1) were transfected with the empty vector (pCDNA) or vectors for the expression of indicated domains of ASAP1 or ACAP1 and were processed for imaging as in Figure 2. **A.** Representative images of the transfected cells. MIPs of cells stained for the epitope tag on the indicated protein and with Phalloidin Alexa Fluor 488 to visualize actin filaments. White open arrowheads indicate thickening of stress fibers at the cell periphery as a result of ASAP1 BAR-PH overexpression, closed white arrowheads indicate thickening of stress fibers and increased intensity induced by full-length ASAP1 overexpression. **B.** Effects of ASAP1 and ACAP1 on cellular F-actin levels. Relative levels of F-actin in cells were estimated by measuring total surface fluorescence of Phalloidin Alexa Fluor 488. The signal was normalized to cell area. **C.** Effect of ASAP1 and ACAP1 on cell shape. The ratio of cell length-to-width was measured as described in Figure 1 as an indicator of cell shape. **D.** Effect of ASAP1 and ACAP1 on cell area. The total area of cells expressing the indicated proteins was measured. *p<0.05, **p<0.01, ****<0.0001, n.s. – not significant, one-way ANOVA with Tukey's post hoc test, n = 10 cells, scale bar = 10 μm, results are presented as mean ± s.e.m. and are a representative of three independent experiments.

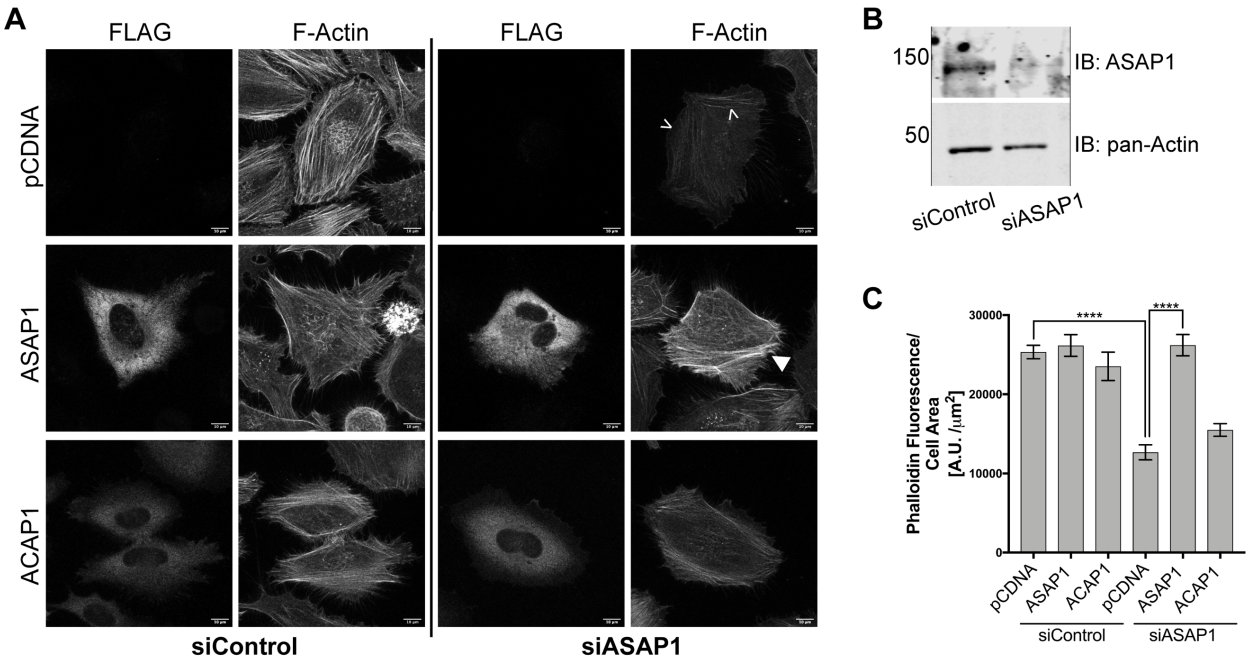

Figure S6. ACAP1 is unable to restore filamentous actin depletion caused by decreased ASAP1 expression, Related to Figure 7.

Human cervical carcinoma cells HeLa were transiently transfected with a control siRNA or siRNA against the 3'UTR region of human ASAP1. After 48 hours, siControl and siASAP1 cells were transfected with empty vector (pCDNA), or pCDNA with the open reading frame for FLAG-tagged full length ASAP1 or ACAP1. 24 hours later (72 hours total), cells were replated on fibronectin-coated coverslips and processed for confocal imaging as before. **A.** Representative images of cells transfected with the indicated siRNA (closed white arrowheads indicating restored stress fibers). **B**. ASAP1 levels in cells treated with control and ASAP1 3'UTR siRNA. ASAP1 was detected by immunoblotting. **C**. F-actin levels in transfected cells. Relative actin levels were estimated by quantifying total Phalloidin Alexa Fluor 488 fluorescence. The signal was normalized to cell area. AU is arbitrary fluorescence unit. Results are presented as mean ± s.e.m. and are representative of three independent experiments, scale bar = 10 μm, n = 15 cells, ****p<0.0001, one-way ANOVA with Tukey's post hoc tests.

Transparent Methods

Cell Culture and Transfection

Primary human foreskin fibroblast cells (HFF-1, pooled population from newborn males) were maintained in DMEM supplemented with 15% heat-inactivated fetal bovine serum, NIH/3T3 clone 7 cells (mouse) and HeLa (human female) were maintained in DMEM supplemented with 10% heat-inactivated fetal bovine serum and 50 μg/mL penicillin/streptomycin.

FLAG (DYKDDDDK) - tagged mouse ASAP1b full-length (1-1090) WT and mutants, BARPZA (1-724), PZA (325-724), BAR (1-338), BAR-PH (1-431), ΔBARPZA (704-1090), ΔBARPH (431-1090), and ΔSH3 (1-1022) were subcloned into pCDNA3.1 (+) vector using EcoRI-NotI restriction sites. FLAG (DYKDDDDK) – or HA (YPYDVPDYA) – tagged human ACAP1 full-length (1-740), BAR-PH (1-377), and ΔBARPH (376-740) were cloned into pCDNA 3.1 (+) using HiFi Assembly (NEB). ACAP1N-ASAP1C chimera, generated by an overlap PCR of human ACAP1 (aa 1-377) and mouse ASAP1b (aa 431-1090), was cloned as an N-terminal FLAG (DYKDDDDK) construct into pCDNA 3.1 (+) using NheI – NotI sites. Clones were verified by Sanger sequencing in CCR Genomics Core (NCI, Bethesda, MD).

For knockdown experiments, cells were transfected with 50 nM siRNAs using JetPrime reagent (Polyplus). Mock-transfected (reagent only) cells and cells transfected with two independent control and two independent ASAP1 siRNAs were used for knockdown experiments. Dharmacon Control #3 and #5 siRNAs were used for mouse cell lines and Dharmacon Control #4 and #5 were utilized for human cell lines.

For rescue experiments, cells were transfected with 50 nM control siRNA or siRNA against 3'UTR region of ASAP1 as done for the knockdown experiments. After 48 hours, cells were transfected with empty pCDNA vector or vector encoding for full-length ASAP1b or ACAP1 using Lipofectamine LTX reagent at 1:3 ratio (DNA : reagent) (Life Technologies). Cells were analyzed 24 hours later (72 hours total).

For overexpression studies, cells were transfected with empty vector plasmid or plasmid encoding full-length and domain truncations of ASAP1 and ACAP1 with Lipofectamine LTX reagent at 1:3 ratio (DNA : reagent). Cells were analyzed after 24 hours.

Recombinant Protein Purification

Protein purification was carried out as described previously (Chen et al., 2016, Jian et al., 2009, Jian et al., 2015) with modifications. Plasmids were transformed into BL21(DE3)-RIL or BL21(DE3) LOBSTR, and grown in LB supplemented with 0.5% glycerol and 1X metals mix and induced with 0.25 mM IPTG overnight at 18°C or grown in auto-induction media for 48 hours at 23°C (Studier, 2005). Cell pellets expressing His_6-tagged constructs were lysed in buffer A (20mM HEPES pH 7.7, 500mM NaCl, 10mM Imidazole) supplemented with protease inhibitors, 0.1% Tween-20, 0.5% sodium deoxycholate using 3 rounds of sonication. Pre-cleared lysates were passed through Ni-NTA (Qiagen) packed gravity column pre-equilibrated with Buffer A and bound His_6-tagged proteins were eluted with Buffer B (20mM HEPES pH 7.7, 500mM NaCl, 250mM Imidazole). After Ni-NTA IMAC purification, ASAP1 PZA was dialyzed against 20mM HEPES 7.7, 200mM NaCl, 0.1% beta-mercaptoethanol overnight, concentrated using Amicon filter and further purified using a Sephacryl S-100 16/60 size exclusion gel filtration column (GE Healthcare). After Ni-NTA elution, ASAP1 BAR-PH and BARPZA were purified on hydroxyapatite column (Bio-Rad), followed by Sephacryl S200 16/60 size exclusion gel filtration without further concentration. GST- tagged SH3 and ΔBARPZA or GST alone were lysed in 1X PBS by passing through cell disruptor (Microfluidics M-110P) three times, followed by addition of Triton X-100 (1% v/v final). Pre-cleared lysates were passed through Glutathione bead packed gravity column (GE Healthcare) equilibrated with lysis buffer, eluted with 20 mM Tris, pH8.0, 100 mM NaCl, 10 mM Glutathione and the elution buffer was exchanged into 1X PBS using PD-10 desalting column. Full-length His_6-tagged ASAP1 was expressed in Sf9 baculovirus (Protein Production Core, Leidos Biomedical Research, Frederick National Laboratory for Cancer Research). Cell pellet was lysed using a Dounce homogenizer in 20 mM HEPES pH7.7, 500 mM NaCl, 5% glycerol, followed by purification using Ni-NTA IMAC and size exclusion gel filtration without concentration.

All chromatography steps were done at room temperature.

Preparation of Large Unilamellar Vesicles (LUVs)

Vesicles (40% phosphatidylcholine (PC), 25% phosphatidylethanolamine (PE), 15% phosphatidylserine (PS), 7.5% phosphatidylinositol (PI), 2.5% PIP_2, and 10% cholesterol) were prepared by extrusion through Whatman Nucleopore 1.0 μm filter, as described previously (Jian et al., 2009).

SDS-PAGE and Immunoblotting

To assess efficiency of knockdown, equal numbers of cells were lysed directly in 2X Laemmli sample buffer + 0.05% beta-mercaptoethanol + protease inhibitors or sonicated in SDS boiling buffer (2.5% SDS, 50mM Tris pH 8.0, 150mM NaCl with protease and phosphatase inhibitor cocktail, modified from (Kovac et al., 2013)), separated by SDS-PAGE (Bio-Rad) and transferred onto nitrocellulose membranes.
For quantitative immunoblotting, after blocking (LI-COR PBS blocking buffer + 0.1% Tween-20), membranes were incubated with primary antibodies diluted in blocking buffer overnight at 4°C. Membranes were washed thrice in PBS + Tween-20 (0.1%) and incubated with fluorophore-conjugated secondary antibodies diluted 1:10,000 in LI-COR blocking buffer in the dark. Membranes were washed thrice in PBS-Tween-20 (0.1%), once in PBS, and scanned using an Odyssey imaging system. Band intensities were determined using Image Studio Lite (LI-COR Biosciences).
For standard X-Ray film-based immunoblotting, after blocking (5% BSA, 0.2% Tween-20 in PBS), membranes were incubated with primary antibodies overnight at 4°C diluted in the blocking buffer. Membranes were washed thrice in PBS + Tween-20 (0.2%) and incubated with HRP-conjugated secondary antibodies at 1:3,000 dilution, washed and processed with ECL reagent.

Immunofluorescence and Confocal Microscopy

Transfected cells were re-plated in a single cell suspension on fibronectin coated #1.5 German glass coverslips in serum-free Opti-MEM for 5.5 hours and fixed in 4% paraformaldehyde (PFA) in PEM (PIPES/ EDTA/ $MgCl_2$) buffer or PBS (Leyton-Puig et al., 2016). For staining with focal adhesion markers, cells were fix-permeabilized on ice in 0.1% Triton-X 100 and 4% PFA in PEM or PBS for 3 min, followed by 4% PFA fix on ice (Cohen et al., 2005). Free aldehydes were quenched with 100 mM Glycine in PBS, and cells were permeabilized and blocked with buffer containing BSA (5% w/v), goat serum (5% v/v), and saponin (0.2% w/v) in PBS for 1 hour, followed by staining with primary antibodies (1 hour in blocking buffer) and fluorescently labeled secondary antibodies and/or fluorescently labeled phalloidin (30 min in buffer containing BSA (1% w/v) and saponin (0.1% w/v)). Coverslips were mounted with DAKO mounting medium. Confocal microscopy was performed on Leica TCS SP8 confocal laser scanning microscope using system optimized z-stack parameters, pinhole = 1.00 Airy Unit, an HC PL APO CS 63x/1.4 oil objective, at 700 Hz with bidirectional X enabled. Data of a given experiment were collected the same day using identical settings. To account for differences in sizes for different cell types, the following parameters were used - NIH/3T3 and HeLa cells, XY = 1024 x 1024 with zoom factor of 1.78 and pixel size of 101.33 x 101.33, for primary HFF-1 cells, XY = 1400 x 1400, with zoom factor of 1.28 and pixel size of 103.45 x 103.45.
Total cell fluorescence and line scan fluorescence were quantified using Imaris (Surface module, whole volume of cell spheroid) and ImageJ/Fiji total fluorescence (on sum of stacks). Approximation of actin filament length and number of stress fibers was done using L Pixel ImageJ plugin Filter2D/ThinLine to extract filaments (on sum of stacks) with length quantified using Ridge Detection Plugin at Sigma 1.50, Lower Threshold 3.00, Upper Threshold 8.00 (Ueda et al., 2010, Steger, 1998) and Filament Sensor using default parameters (Eltzner et al., 2015).

In Vitro Actin Binding and Bundling Assay

Two sources of rabbit skeletal muscle actin were used: (i) filamentous actin prepared from rabbit skeletal muscle as described (Pardee and Spudich, 1982) and; (ii) G-actin purchased from Cytoskeleton, Inc. G-actin was polymerized to F-actin according to the manufacturer's protocol and efficiency of polymerization was assessed by sedimentation at 120,000 x g, followed by SDS-PAGE of the pellet (F-actin) and the supernatant (G-actin) fractions. High- and low- speed actin co-sedimentation assays were performed according to the manufacturer's protocol (Cytoskeleton, Inc.). Prior to performing the assays, all test proteins were spun at 150,000 x g for 1 hour at 4°C to sediment aggregates and particulates. For F-actin binding experiments (high-speed cosedimentation), test proteins (2 μM) were incubated with varying concentrations of F-Actin (0 – 25 μM) in F-actin buffer (5 mM Tris pH 8.0, 50 mM KCl, 2 mM $MgCl_2$, 0.2 mM $CaCl_2$, 1 mM ATP) for 30 min and centrifuged at 150,000 x g for 90 min at 24°C in Thermo Scientific Sorvall MTX150 ultracentrifuge. For F-actin bundling experiments (low-speed centrifugation), test proteins were incubated with F-actin as before and centrifuged at 14,000 x g for 30 min at 24°C in a tabletop centrifuge (Eppendorf 5415R). For both assays, equal amounts of supernatant and pellet fractions were separated on SDS-PAGE, stained with GelCode Blue stain and quantified using ImageJ or Image Studio Lite software.

For fluorescence-based actin bundling assays, reactions were prepared as for co-sedimentation assays and spotted in 2-5 μL drops on poly-L-Lysine covered coverslips. Coverslips were fixed on ice with 4% paraformaldehyde in PBS and stained with Rhodamine Phalloidin on ice, mounted and imaged on Leica TCS SP8 as above (Lin-Jones and Burnside, 2007). For immune-localization of ASAP1 BAR-PH on actin bundles, samples were incubated with 1% BSA and 3 μM phalloidin after fixation to stabilize filaments, followed by primary antibody incubation (1:500), three PBS washes and incubation in fluorescently-labeled secondary antibody and phalloidin (Yamada et al., 2016, Yamada et al., 2013).

In Vivo F-Actin/ G-Actin Assay

NIH/3T3 fibroblasts were transfected with a control or siASAP1 siRNA for 72 hours, plated on fibronectin-coated 6-well plates for 6 hours and processed according to the protocol for adherent cells using G-Actin/ F-Actin In Vivo Assay Kit (Cytoskeleton). Cells were lysed in prewarmed lysis buffer (LAS2, 37°C), homogenized using trituration and incubated for 10 min at 37°C. Crude lysate (100 μL) was reserved for BCA protein quantification assay. The rest of the lysate (~400 μL) was pre-spun at 360 x g to remove unbroken cells, divided equally into four ultracentrifuge tubes and centrifuged at 100,000 x g in pre-warmed ultracentrifuge (Thermo Scientific Sorvall MTX150). Equal amounts of supernatant (G-actin) and pellet (F-actin) fractions were separated on SDS-PAGE and F- to G-actin ratios and F-actin content were analyzed using quantitative LI-COR immunoblotting. GAPDH was used as a loading control. Efficiency of knockdown was confirmed on a separate immunoblot using standard ECL.

Stress Fiber Extraction

Stress fiber extraction from human foreskin fibroblasts was performed as described (Katoh et al., 2000). 72 hours post-transfection with siRNAs, cells were incubated in serum-free media on fibronectin-coated coverslips for 5.5 hours. Cells were briefly washed with ice-cold PBS, followed by 10-20 washes in low-ionic strength solution (2.5 mM triethanolamine, TEA) to remove dorsal side of the cells. Remnants of the dorsal components as well as nuclei were removed with Extraction buffer I (0.05% NP-40 in PBS), followed by a brief wash in Extraction Buffer II (0.5% Triton-X 100 in PBS). The remaining detergent was removed by triple washing with PBS. All buffers were supplemented with protease inhibitors and all steps were done on ice with continuous rocking. Extracted stress fibers were fixed and processed for confocal microscopy analysis as before.

Proteolysis Protection Assay

Proteolysis protection assay was performed according to (Fievez and Carlier, 1993), with the following modifications. Briefly, for F-actin-mediated protection, purified full-length recombinant ASAP1 (1 mg/mL) was incubated with F-actin (0.5 mg/mL) in F-actin buffer (5 mM Tris HCl, pH 7.5, 50 mM KCl, 2 mM $MgCl_2$, 1 mM ATP, 0.5 mM DTT) and subjected to protease digestion with Subtilisin A (1 μg/mL) at 25ºC. Aliquots were taken out at the indicated time points, quenched with PMSF and EDTA (1 mM each final), and boiled in 4X Laemmli sample buffer. Digestion of ASAP1 alone and F-actin alone were performed simultaneously as controls. For G-actin-mediated protection, experiments were done as before, but using G-actin and general actin buffer (5 mM Tris, pH 8.0, 0.2mM $CaCl_2$, 0.2 mM DTT). Samples were separated by SDS-PAGE and stained with GelCode Blue.

For determination of regions protected by interaction with F-actin, 0, 5, and 15 min time points were subjected to quantitative immunoblotting (LI-COR) using ASAP1 antibodies raised to C-terminal (antiserum 642) and N-terminal (antiserum 645) antigens.

Statistical Analysis

Statistical analyses were carried out using SigmaPlot and GraphPad Prism. Comparison of two groups was carried out using Student's t-test, and comparison of data sets with more than two groups was carried out using ANOVA with multiple comparisons. Alpha was set to 0.5 for all experiments. Values represented are mean ± s.e.m., unless otherwise noted. For figures describing cell biology experiments, "n" indicates number of cells per group per experiment, unless otherwise noted.

Key Resources Table

REAGENT or RESOURCE	SOURCE	IDENTIFIER
Antibodies		
mouse anti-FLAG tag	Cell Signaling Technology	#8146; RRID:AB_10950495
rabbit anti-FLAG tag	Cell Signaling Technology	#14793
mouse anti-HA tag	BioLegend	#901501
mouse anti-His_6 tag	Invitrogen	#37-2900
rabbit anti-pan Actin	Cell Signaling Technology	#8456; RRID:AB_10998774
mouse anti- paxillin clone 349	BD Biosciences	#610052
mouse anti-vinculin, clone hVin-1	Sigma-Aldrich	#V9131
mouse anti-HSC70	Santa Cruz	#sc7298
rabbit anti-pan-Actin	Cytoskeleton, Inc.	#AAN01-A
rabbit anti-ASAP1 642 C-terminal epitope (VELAPKPQVGELPPKPGC)	Randazzo Lab	(Randazzo et al., 2000)
rabbit anti-ASAP1 645 N-terminal epitope (DQDRTALQKVKKSVAC)	Randazzo Lab	(Randazzo et al., 2000)
mouse anti-ASAP1	Abnova	#H00050807-M01
mouse anti-GAPDH	Millipore	#CB1001
mouse anti-alpha Tubulin	Invitrogen	#A-11126
Alexa Fluor 488 goat anti-mouse IgG (H+L)	Invitrogen	#A-11001
Alexa Fluor 488 goat anti-rabbit IgG (H+L)	Invitrogen	#A-11008
Alexa Fluor 594 goat anti-mouse IgG (H+L)	Invitrogen	#A-11032
IRDye 680RD goat anti-mouse	LICOR	#926-68070
IRDye 800CW donkey anti-rabbit	LICOR	#926-32213
anti-rabbit HRP IgG	Bio-Rad	#1706515
Chemicals, Peptides, and Recombinant Proteins		
Alexa Fluor 488 Phalloidin	Invitrogen	#A-12379
Rhodamine Phalloidin	Invitrogen	#R415
Alexa Fluor 594 Phalloidin	Invitrogen	#A-12381
Alexa Fluor 647 Phalloidin	Invitrogen	#A-22287
Lipofectamine LTX	Invitrogen	#15338-100
JetPRIME transfection reagent	Polyplus transfection	#114-07
Fibronectin	Sigma-Aldrich	#F1141
16% Paraformaldehyde Solution	Electron Microscopy Sciences	#15710
Saponin	Sigma-Aldrich	S7900
Bovine Serum Albumin	Sigma-Aldrich	A7906
Normal goat serum	Abcam	#ab7481
Subtilisin A	Sigma-Aldrich	#P5380-250mg
Poly-L-Lysine	Sigma-Aldrich	#P4707
Actin, rabbit muscle, globular form	Cytoskeleton	#AKL99
Actin, rabbit muscle, filamentous form	Sellers Lab (NIH, Bethesda, MD)	(Collins et al., 1991)
alpha-actinin, rabbit muscle	Cytoskeleton, Inc.	#AT01

Fluorescence Mounting Medium	DAKO	#S3023
phosphatidylcholine, PC, chicken egg	Avanti Polar Lipids	#840051
phosphatidylethanolamine, PE, bovine liver	Avanti Polar Lipids	#840026
PI(4,5)P_2, porcine brain	Avanti Polar Lipids	#840046
phosphatidylinositol, PI, bovine liver	Avanti Polar Lipids	#840042
phosphatidylserine, PS, porcine brain	Avanti Polar Lipids	#840032
Cholesterol, ovine wool	Avanti Polar Lipids	#700000
Critical Commercial Assays		
Actin Binding Spin Down Assay Kit	Cytoskeleton, Inc.	#BK001
G-Actin/ F-Actin In Vivo Assay Biochem Kit	Cytoskeleton, Inc.	#BK037
Bacterial and Viral Strains		
Primary HFF-1	American Type Culture Collection	#SCRC-1041
HeLa	Randazzo Lab	N/A
NIH/3T3 clone 7	Douglas Lowy Lab (NCI/NIH, Bethesda, MD)	N/A
Experimental Models: Organisms/Strains		
BL21 (DE3) CodonPlus-RIL	Agilent	#230245
LOBSTR BL21 (DE3) RIL	Kerafast	#EC1002
NEB5alpha	New England Biolabs	#C2987I
Oligonucleotides		
Non-targeting control #3	Dharmacon	D-001210-03-20
Non-targeting control #4	Dharmacon	D-001210-04-05
Non-targeting control #5	Dharmacon	D-001210-05-50
siGENOME Human ASAP1 siRNA CDS #2	Dharmacon	D-031961-02-0050
siGENOME Human ASAP1 siRNA CDS #17	Dharmacon	D-031961-17-0050
Accell Human ASAP1 siRNA 3'UTR #16	Dharmacon	A-031961-16-0005
siGENOME Mouse ASAP1 siRNA CDS #2	Dharmacon	D-040558-02-0050
siGENOME Mouse ASAP1 siRNA 3'UTR Sense: 5' GCAUGCAUCUAGACGCUUAUU 3'	Dharmacon	Custom synthesis
Recombinant DNA		
ASAP1 BAR-PH-His_6 (aa 1-431) (pET21a)	Randazzo Lab	(Jian et al., 2009)
ASAP1 BARPZA-His_6 (aa 1-724) (pET21a)	Randazzo Lab	(Jian et al., 2009)
ASAP1 PZA-His_6 (aa 325-724) (pET21a)	Randazzo Lab	(Jian et al., 2009)
mASAP1 full-length (1-1090) (pDEST8)	Leidos Biomedical Research	N/A
GST ASAP1 ΔBARPZA (724-1090) (pGEX-4T)	This paper	N/A
GST ASAP1 SH3 (997-1090) (pGEX-4T)	This paper	N/A
FLAG mASAP1b full-length (pCDNA 3.1 (+))	This paper	N/A
FLAG ASAP1 BAR-PH (pCDNA 3.1 (+))	This paper	N/A
FLAG ASAP1 BARPZA (pCDNA 3.1 (+))	This paper	N/A
FLAG ASAP1 ΔSH3 (pCDNA 3.1 (+))	This paper	N/A
FLAG ASAP1 ΔBARPH (pCDNA 3.1 (+))	This paper	N/A
FLAG ASAP1 ΔBARPZA (pCDNA 3.1 (+))	This paper	N/A
FLAG or HA ACAP1 BAR-PH (pCDNA 3.1 (+))	This paper	N/A

FLAG or HA ACAP1 ΔBARPH (pCDNA 3.1 (+))	This paper	N/A
FLAG or HA ACAP1 full-length (pCDNA 3.1 (+))	This paper	N/A
Software and Algorithms		
Imaris Software	8.1 Bitplane	http://www.bitplane.com/imaris/imaris
Fiji		https://fiji.sc/
ImageJ	National Institutes of Health	https://imagej.nih.gov/ij/
SigmaPlot 12.5	Systat Software, Inc.	https://systatsoftware.com/products/sigmaplot/sigmaplot-product-updates/
Prism v7.7	GraphPad	https://www.graphpad.com/scientific-software/prism/
Ridge Detection Plugin	ImageJ plugins	https://imagej.net/Ridge_Detection
Line Filter Plugin	L Pixel (Hasezawa Lab, University of Tokyo)	https://lpixel.net/en/products/lpixel-imagej-plugins/
Filament Sensor	Florian Rehfeldt Lab, University of Göttingen	(Eltzner et al., 2015)
Other		
#1.5 German coverslip 18mm	Electron Microscopy Science	#72292-10
Opti-MEM	Gibco	51985091
DMEM	Gibco	11965118
Penicillin/ Streptomycin	Gibco	15140122
Fetal Bovine Serum	Gibco	10437028

Supplemental References

COHEN, D. M., CHEN, H., JOHNSON, R. P., CHOUDHURY, B. & CRAIG, S. W. 2005. Two distinct head-tail interfaces cooperate to suppress activation of vinculin by talin. *J Biol Chem,* 280**,** 17109-17.

COLLINS, K., SELLERS, J. & MATSUDAIRA, P. 1991. Myosin I: a new insight into the mechanism and cellular significance of actin-based motility. *Adv Biophys,* 27**,** 221-6.

JIAN, X., TANG, W. K., ZHAI, P., ROY, N. S., LUO, R., GRUSCHUS, J. M., YOHE, M. E., CHEN, P. W., LI, Y., BYRD, R. A., XIA, D. & RANDAZZO, P. A. 2015. Molecular Basis for Cooperative Binding of Anionic Phospholipids to the PH Domain of the Arf GAP ASAP1. *Structure,* 23**,** 1977-88.

LEYTON-PUIG, D., KEDZIORA, K. M., ISOGAI, T., VAN DEN BROEK, B., JALINK, K. & INNOCENTI, M. 2016. PFA fixation enables artifact-free super-resolution imaging of the actin cytoskeleton and associated proteins. *Biol Open,* 5**,** 1001-9.

PARDEE, J. D. & SPUDICH, J. A. 1982. Purification of muscle actin. *Methods Enzymol,* 85 Pt B**,** 164-81.

STEGER, C. 1998. An unbiased detector of curvilinear structures. *Ieee Transactions on Pattern Analysis and Machine Intelligence,* 20**,** 113-125.

STUDIER, F. W. 2005. Protein production by auto-induction in high density shaking cultures. *Protein Expr Purif,* 41**,** 207-34.

UEDA, H., YOKOTA, E., KUTSUNA, N., SHIMADA, T., TAMURA, K., SHIMMEN, T., HASEZAWA, S., DOLJA, V. V. & HARA-NISHIMURA, I. 2010. Myosin-dependent endoplasmic reticulum motility and F-actin organization in plant cells. *Proc Natl Acad Sci U S A,* 107**,** 6894-9.